# Chapter 1
# Introduction

This chapter offers a background of temperature impact on energy efficiency of solar cell module and methods for reducing the solar cell module temperature. The application of phase change material for controlling the solar cell module temperature is described.

## 1.1 Background and Statement of Problems

Every year, the world energy demand increases gradually as given in Figure 1.1 and the main primary world energy consumption comes from the fossil fuels which are the limited resources. In 2014, fossil fuels represented for 86% of total primary energy consumption and hydro and other renewables energy shared about 10% [1]. Carbon dioxide goes into the atmosphere by burning oil, natural gas and coal. According to BP Global statistics [2], 35 billion tonnes of $CO_2$ was released to the environment in every year. In 2014, the $CO_2$ represented about 80% of greenhouse gases that made earth warming by trapping heat in the atmosphere. This problem can be alleviated by replacing fossil fuel by renewable energy.

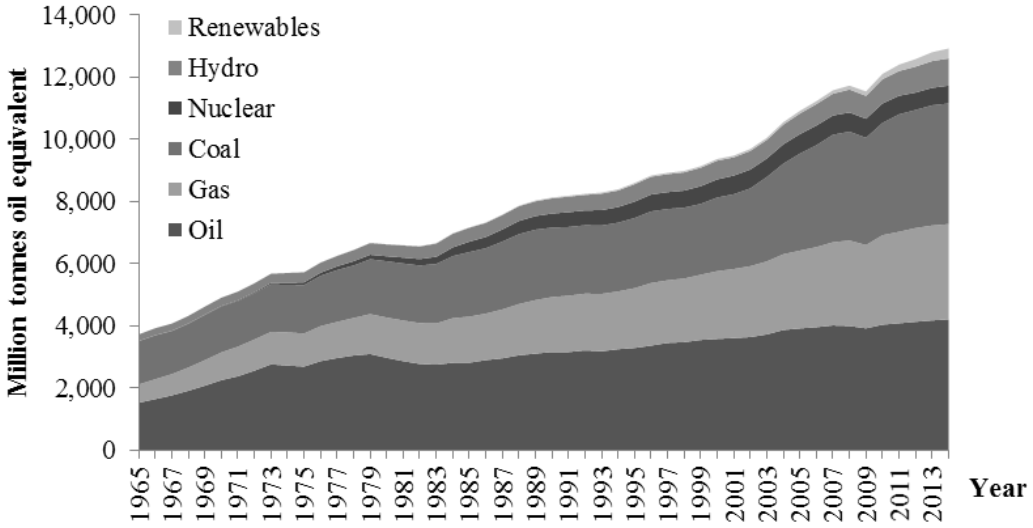


Figure 1.1 Primary world energy consumption 1965-2014 [1].

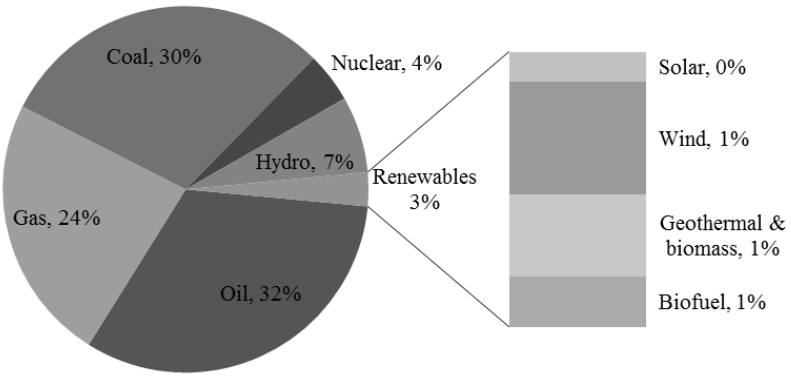


Figure 1.2 Total energy consumed in 2014 [1].

Nowadays, the solar cell is one type of renewable equipment that has a huge market as shown in Figure 1.3 (Renewables 2014 Global Status Report). Since 2011, about 30 GW electricity of solar cell has been installed every year [3]. In 2014, the top three markets were China, Japan, and the United States, followed by the United Kingdom and Germany. China added 10.6 GW of global total capacity 28 GW in 2014.

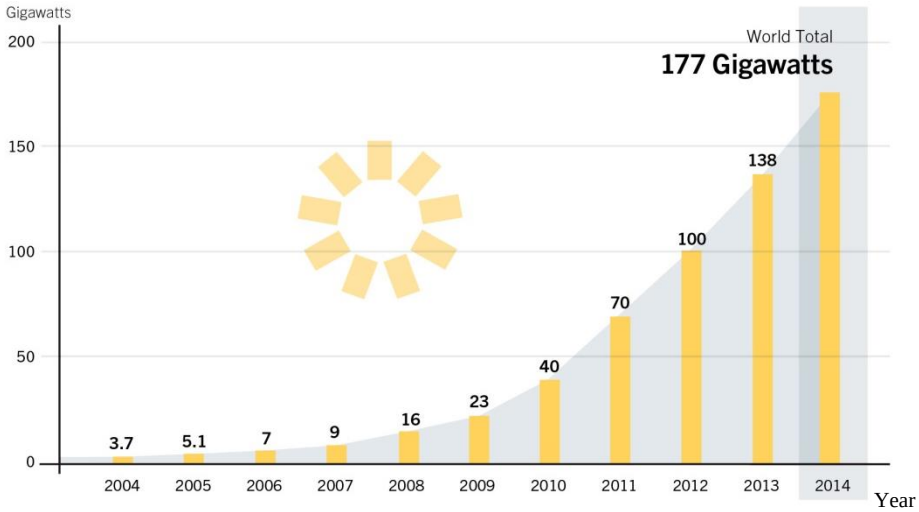


Figure 1.3 Solar cell global capacity, 2014 [3].

Solar cell is an electricity generating component that converts sunlight into electricity directly as illustrated in Figure 1.4. When sunlight (photons) strikes on a PV cell, an electrical current is produced by stimulating electrons (negative charges) in the cell layer and some electrons could move to another layer. The layers those have difference electrons will generate the electric field. When positive and negative sides are connected to an external load, there will be a movement of electrons thus electrical current could be generated.

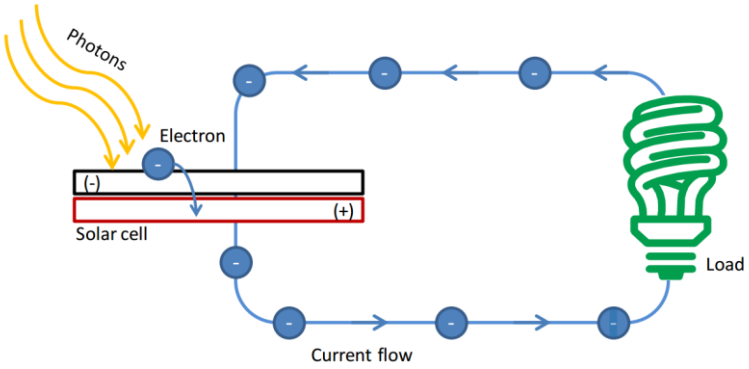


Figure 1.4 A circuit of electrical generation from solar cell [4].

Currently, there are 3 types of solar cell. The first one is solar cells made of crystalline silicon which is commonly designed as flat-plate and this one gives the highest efficiency. The second type is made of amorphous or non-silicon material such as cadmium telluride. The solar cells are flexible but the efficiency is rather low. For the third type is called Emerging PV that are made of new materials besides silicon such as: copper zinc tin sulfide, organic solar cell, dye-sensitized solar cell, Perovskite solar cell, Polymer solar cell, and Quantum dot solar cell. The crystalline silicon solar cells are the most common units in use today. They have a long lifespan in a range of 25–30 years and they can keep producing energy beyond this range [4]. The overall efficiency of the most silicon solar cells is between 12% and 18%. According to Martin et al., mono-crystalline silicon cell and poly-crystalline silicon cell has highest efficiency 25.6 ± 0.5% and 20.8 ± 0.6% respectively [5].

As mention above the silicon solar cells are most common available in the market. The efficiency could be obtained under standard testing condition at solar irradiance of 1,000W/m$^2$, air mass 1.5 and the operating temperature of the module is maintained at 25 °C. However, in the real practice, the solar radiation is varying depends on the sun path and cloud condition. The operating temperature of the module solar cell will be hotter than 25 °C, especially in the hot country like Thailand of which the ambient temperature is sometimes over 40 °C and the maximum temperature of module might reach 70 °C then the generated power and the conversion efficiency of the solar cell will be less than those at the standard condition.

Several techniques, like water cooling and air cooling, are used to control the solar cell module temperature and these are described in the literature review.

In this study, phase change material (PCM) is coupled at the back of solar cell module to absorb the heat energy from the solar cell by its latent heat and sensible heat. This technique is able to reduce the solar module temperature without any external power.

## 1.2 Literature Review

### 1.2.1 The Temperature Influence on Power Output of Solar Cell

Figure 1.5 shows the optimum efficiency of solar cell as a function of bandgap energy and temperature. Landis et al. proposed a model of a solar cell at high operating module temperature, high intensity of solar radiation condition. The optimum band gap shifted from 1.4 V at room temperature of 27 °C to 2.3 V at 900 °C. The increase of cell temperature also increased optimum bandgap energy but dropped the solar cell efficiency [6].

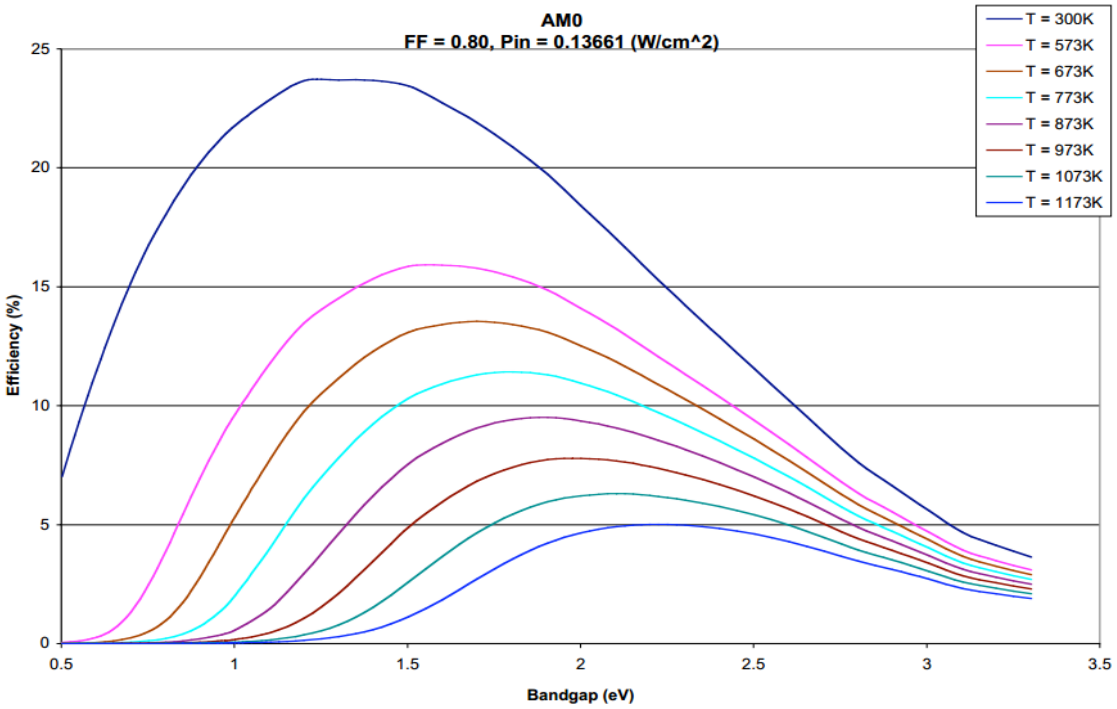


Figure 1.5 Theoretical efficiency of a solar cell as a function of bandgap and high temperature [6].

When the operating module temperature increases, the open circuit voltage (Voc) drops with a little increase in short circuit current (Isc) as illustrated in Figure 1.6; the wattage of electrical energy output also decreases [7].

The peak power output of solar cell is given by the standard testing with a solar radiation of 1,000 W/m$^2$ and the cell temperature is maintained at 25 °C. But in real operating condition, the solar radiation is varying with time during a day and the operating cell temperature is normally over than 25 °C then the generated power and the conversion efficiency of the solar cell will be less than those at the standard condition.

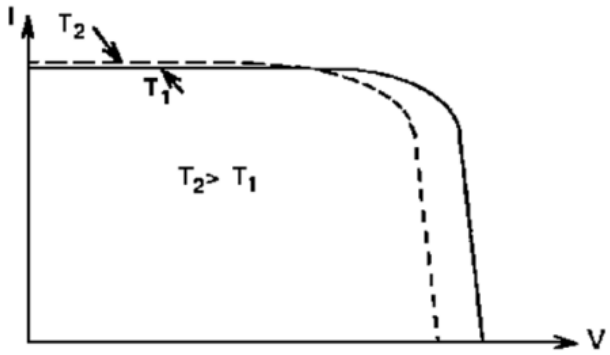


Figure 1.6 Curve in difference solar cell module temperature.

The influences of temperature and solar spectrum wavelength on the performance of crystalline solar cell module were reported by [8] and the solar cell module was heated up to 80°C; Radziemska founded that the power output was decreased 0.65% per degree Celsius.

1.2.2 Cooling Methods

Several techniques, such as water cooling and air cooling, were applied to reduce the operating temperature of the solar cell modules. Abdozadeh and Ameri [9] used water spray over the front of solar cell module. This technique could maintain the temperature of the solar module close to the ambient temperature but some part of the electrical power was mainly used for water pumping. The uses of forced air cooling techniques were discussed by Teo et al. [10] and Asanakham et al. [11]. With the air blower, the operating module temperature could be maintained at 38 °C and without cooling at 68 °C. It could be seen that both of water and air cooling techniques required the external power for running the pump and fan.

Figure 1.7 Cooling solar cell by water flow [9].

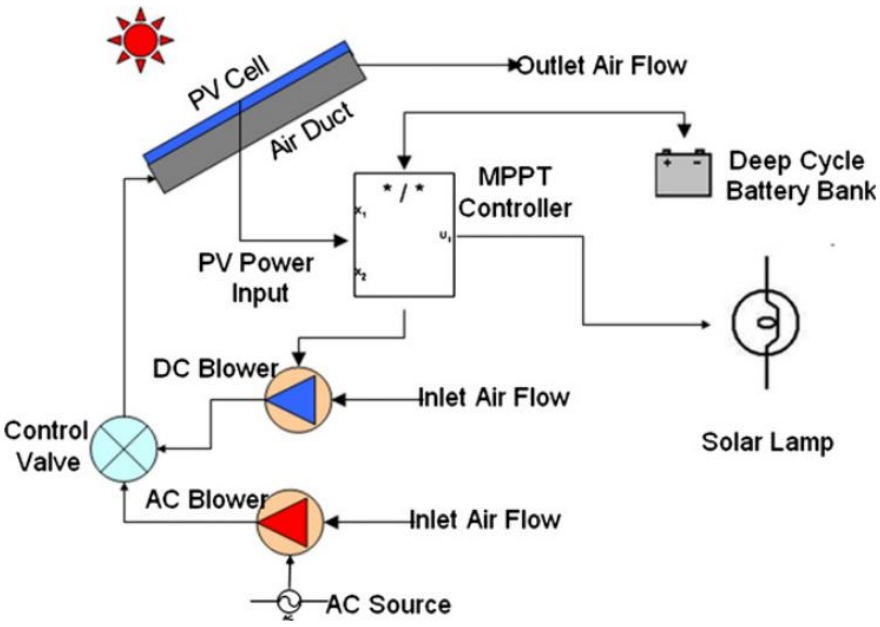


Figure 1.8 PV cooling by air [10].

1.2.3 Phase Change Materials

Phase Change Materials (PCMs) are substances that contain large amounts of energy storage capacity with a small of temperature range due to the phase transitions with large latent heats. Generally, latent heat energy storage can be achieved through solid-liquid, liquid-gas, or solid-gas phase change. In normal applications, the solid-liquid phase transition is mostly used [12].

Figure 1.9 shows relationship between PCM's melting temperature and enthalpy for different kinds of PCMs. Paraffins, fatty acids and sugar alcohols are organic materials with temperature between 0 and 130 °C. Water-salt usually use for the temperatures below 0 °C. Salt hydrates, inorganic materials, contain a large volumetric latent heat storage capacity [13].

A review on phase change materials for thermal energy storage application and low temperature solar thermal applications has been done by Riffat, et al [14] and Sharma et al. [15], respectively.

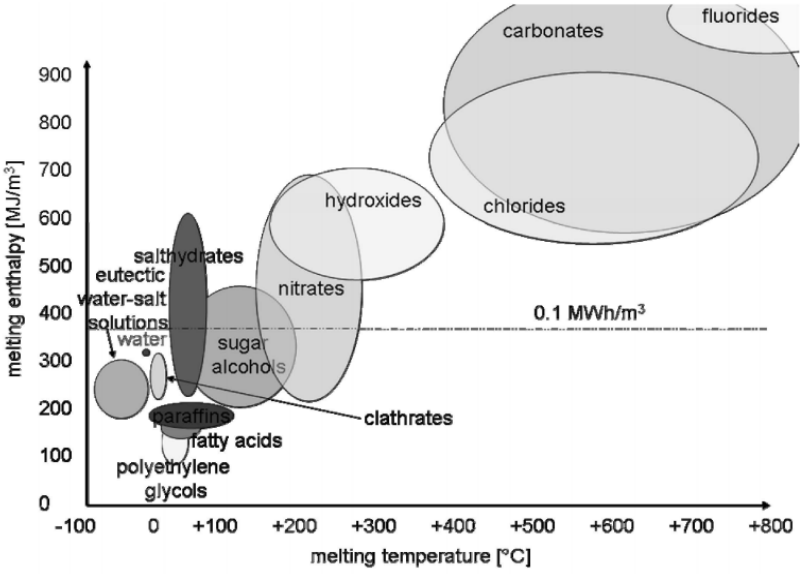


Figure 1.9 PCM and their typical range of point and enthalpy (picture: ZAE Bayern).

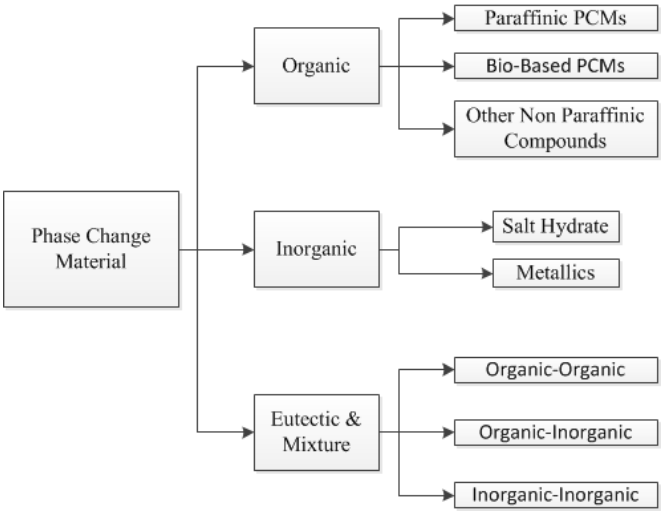


Figure 1.10 Classification of PCMs [14].

PCMs were classified by Riffat et al. and Abhat [14,16] and the available materials into organic, inorganic and eutectic materials as show in Figure 1.10.

Some PCMs have the low thermal conductivity around 0.2-0.6 W/m K, such as paraffin wax, salt hydrates and eutectic [17]. For improving the thermal conductivity, metal or graphite in form of powders or fibers was added to PCM. A disadvantage of metals is corrosive and its stability in high temperature, especially when they combine with water, water-salt, salt or salt-hydrates solutions [13].

In recent years, the using of PCM for heating and cooling of buildings are very interesting. Thermal analysis of a building brick containing PCM was done by Alawadhi [18].

The heat gain in the building was reduce when brick was incorporated with PCM and the heat flux at indoor space was reduce 17.55%. The integrated PV and PCM into the Double Skin Façade of the building has been studied; 20 to 30% of the cooling energy demand was reduced [19].

Studies on a use of PCM to reduce the PV module temperature have also been presented. There was a study of RT25 PCM installed at the back of a building integrated PV (BiPV) to maintain the module temperature [20]. The melting temperature of the PCM was 26.6 ºC and the temperature of the solar cell module was maintained lower than 29 °C for 2 hours under the solar radiation of 750 W/m2 and the ambient temperature of 23 °C. Similar experiment was also operated under the europe weather condition [21]. The solar cell module temperature could be maintained at the operating temperature less than 40 °C about 2 hours at the solar radiation of about 1,000 W/m2.

PCM also used in Building Integrated Concentrated Photovoltaic for improving the solar cell efficency and redcing the heat gain into the building [22]. Studies presented that PCM effectiveness varies with solar radiation; electrical efficiency were increased 1.15, 4.20 and 6.80% at 500, 750 and1200 W/m2, respectively.

1.2.4 Numerical methods

Several computing program and computation methods in solving heat transfer in PCM were. Sadasivam et al. also used effective heat capacity and enthalpy method for solving heat transfer in PCM but in this case he used Crank-Nicholson with iterative method [23]. Explicit discretization was developed by Heim and Clarle [24] and Kuznik et al. [25]. The enthalpy method is given more accuracy result than effective heat capacity with the small temperature range of phase change [26].

In this study, phase change material (PCM) is coupled at the back of solar cell module to absorb the heat energy from the solar cell by its latent heat and sensible heat. This technique is able to reduce the solar module temperature without any additional power. With the PCM, the solar cell module temperature will decrease and more electrical power will obtain. The series of commercial PCM Rubitherm (RT): RT35, RT42, RT47 and RT55 PCMs with melting temperatures range of 29-36, 38-43, 41-48 and 51-57 °C were taken. Numerical simulation was carried out to find the suitable thickness for each PCM. Experimental study was also performed to verify the numerical study with the module with RT42 PCM. The correlation of power output of solar cell as function of solar radiation and its module temperature is found. The unit cost of the electricity generates by solar cell under the Chiang Mai weather condition is carried out.

## 1.3 Objectives

1.3.1 To investigate the effect of PCM on reduction of the solar cell module temperature for increasing the electrical generation.

1.3.2 To define the appropriate thickness of PCM for cooling the solar cell module.

1.3.3 To estimate the unit cost of solar cell with the PCM system.

## 1.4 Expecting Benefit

1.4.1 A new technique to improve solar cell module performance for generating more electrical power is developed.

1.4.2 Suitable size of the PCM for reducing the solar cell module temperature could be found out.

## 1.5 Scope of Study

1.5.1 The experiment will be done under the climate of Chiang Mai with latitude 18°47′North.

1.5.2 Two identical polycrystalline solar cell modules (EMS250-156 model) are used and each maximum power output is 250 W at the standard condition. Each EMS250-156 module consists of 60 cells and each cell has a size of 156 mm x 156 mm.

1.5.3 The phase change material RT42 is used in this experiment. The properties are as follows: the melting temperature is 38-43 °C, the specific latent heat is 144 kJ/kg, the specific heat capacity is 2 kJ/kg-K, and the thermal conductivity is 0.2 W/m-K. The organic RT42 PCM is selected due to many conditions such as: the high specific latent heat, melting temperature range 38-43 °C is close to the ambient temperature in Thailand, low-volume expansion, non-fatal material and available on the market.

# Chapter 2
# Theory

In this chapter, the controlled module temperature of solar cell by phase change material is first described with its potential of latent heat during the phase change. The numerical method was used for predicting the PCM temperature.

## 2.1 Introduction the Concept of Using PCM for Reducing Solar Cell Module Temperature

To understand the concept for controlling module PV temperature with PCM, the overview of the thermal energy storage is described in this section.

The method of storage has two main processes which are: physical and chemical processes as given in Figure 2.1. The latent heat of phase change is the main core of physical energy storage.

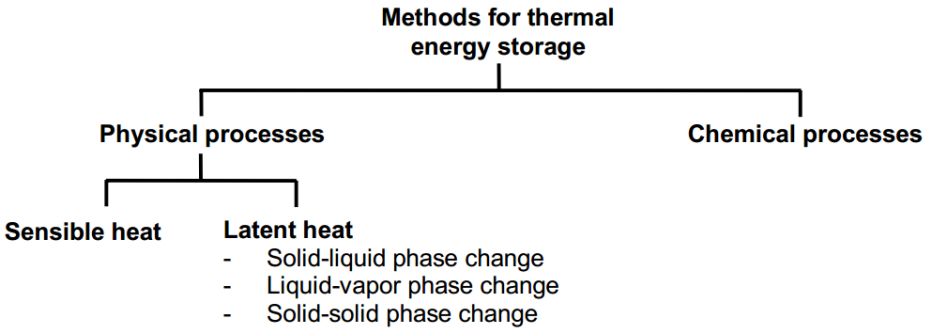


Figure 2.1 Heat and cold storage method [13].

### 2.1.1 Potential of Latent Heat Storage Capacity in Solid-Liquid Phase Transition

The difference of energy change during the phase change process is called latent heat. The latent heat is all so called: melting enthalpy, phase change enthalpy or latent heat of fusion. Within latent heat, the PCM can store large amount of heat energy if the desirable temperature application and suitable PCM are selected.

The energy storage by PCM is shown in Figure 2.2(b). At first, it stores the energy in the solid phase by sensible heat after the temperature reaches the melting temperature. When the melting completes, the sensible heat happens again in the liquid phase.

During melting, the PCM temperature is nearly constant enthalpy change could be used to estimate the energy content in the material thus the enthalpy method for the calculation is used and the further review is presented in section 2.2.

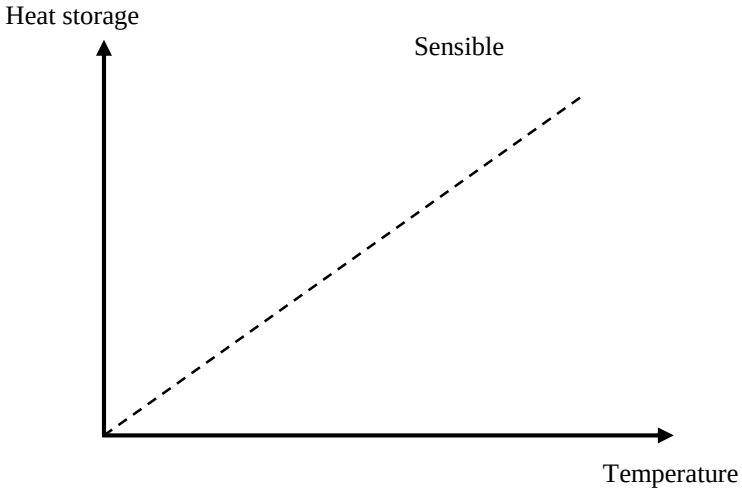


a

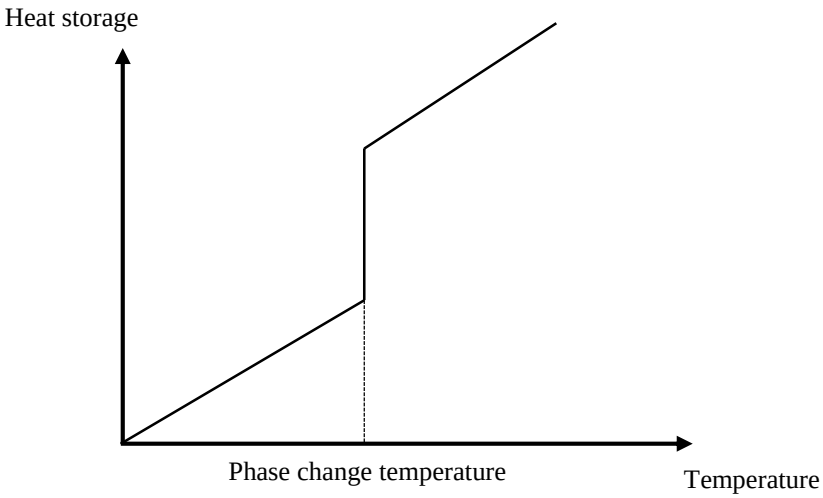


b

Figure 2.2 Heat storage as sensible heat (a) and latent heat in case of solid-liquid phase change (b).

2.1.2 Phase Change Material Selection

The PCM is selected as a thermal storage in many applications and the guideline to select the material is listed below:

Thermo-physical Properties

- The melting/solidification point at temperature desirable application.
- High specific latent heat.
- Small volume change during the phase transition.
- High thermal conductivity in both solid and liquid phases.
- High specific heat capacity in solid or/and liquid phase.

Kinetic Properties

- Non-flammable, non-explosive and non-toxic material.
- No corrosive effect with the construction material.
- No degradation after many cycles of operation.

Economic requirements

- Low price.
- Good recyclability.

### 2.1.3 Potential of PCM for Controlling PV Module Temperature

The solar cell module is consisting of materials such as: silicon, coating glass and Tedlar with the volumetric capacities of 1.5 MJ/m$^3$-K which is about one-third of water. With lowing heat capacity per volume and the thickness is very thin, after exposing to the sun around noon, the solar cell module might reach 70 °C under Thailand climate. With PCM cooling, during the phase transition, the PCM can absorb the heat from the module and control the module temperature to be close to its melting point.

As illustrated in Figure 2.3, the solar cell module temperature reaches the peak temperature around noon. With the PCM, the solar cell module temperature can be reduced the peak due to the latent heat of PCM.

Table 2.1 Heat capacity and heat store in 5°C for different PV material, water and RT42 PCM.

| Material | $c_P$ per mass [kJ/kg-K] | density [kg/m$^3$] | $c_{Pv}$ per volume [MJ/m$^3$-K] | Q/V for ΔT=5°C [MJ/m$^3$] |
|---|---|---|---|---|
| Silicon PV cell | 0.677 | 2330 | 1.577 | 7.89 |
| Tedlar | 1.25 | 1200 | 1.5 | 7.5 |
| Coating | 0.5 | 3000 | 1.5 | 7.5 |
| Water | 4.18 | 1000 | 4.18 | 16.72 |
| RT42 PCM (38-43°C ) | 37 (peak value) | 880 | 32.56 | 126.72 |

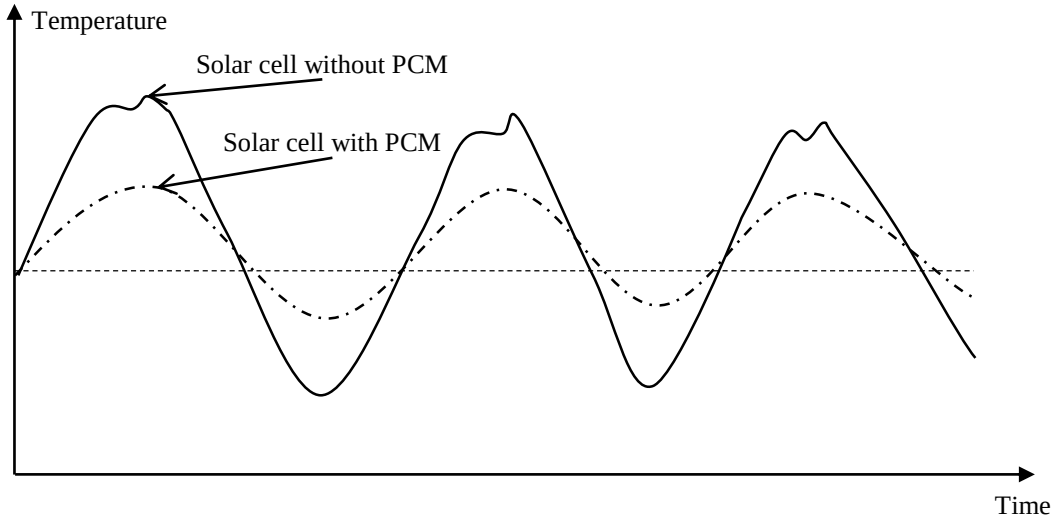


Figure 2.3 Temperature control of solar cell by PCM.

## 2.2 Relation between Enthalpy and Temperature

Enthalpy method is the best method for solving the heat transfer problem in solid state and liquid state and even in phase transition concurrently. The relation of enthalpy with temperature is shown in Figure 2.4. For a pure substance like ice-water, the enthalpy change at the specific melting temperature is shown in the Figure 2.4(a). Figure 2.4(b) shows the relationship of enthalpy with temperature for non-isothermal phase change and the melting temperature is not constant.

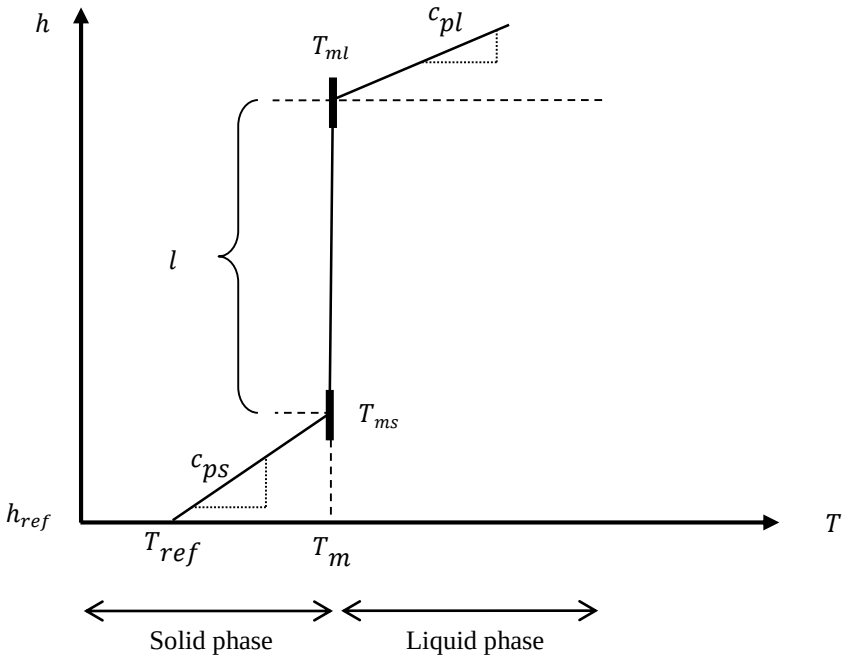


a. The isothermal phase change

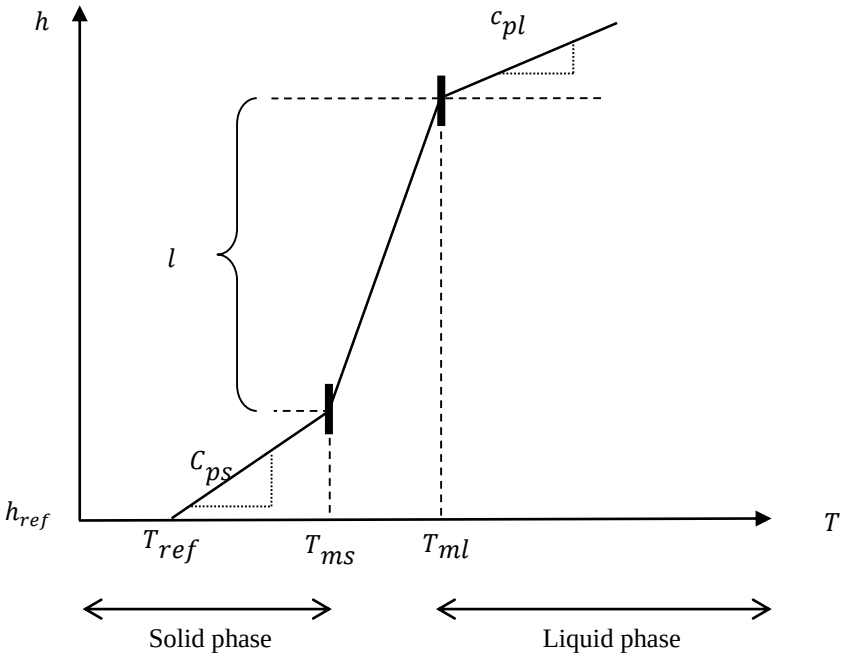


b. Non-isothermal phase change.

Figure 2.4 Enthalpy and temperature relationships: (a) is isothermal and (b) is non-isothermal.

For the numerical simulation, it is essential to know the relation between enthalpy and temperature. The heat capacity $c$ and the latent heat of fusion $l$ are given by the manufacturer or from the literature. In case of pure substance or isothermal phase change, $T_{ms} = T_{ml} = T_m$ as given in Figure 2.4(a) and the enthalpy v.s. temperature could be

$$h = \begin{cases} c_{ps}(T - T_{ref}), & T < T_m \\ c_{ps}(T_m - T_{ref}) + \mathrm{g} \cdot l, & T = T_m \\ c_{ps}(T_m - T_{ref}) + l + c_{pl}(T - T_m), & T > T_m. \end{cases} \tag{2.1}$$

Conversely, the temperature is determined by

$$T = \begin{cases} T_{ref} + h/c_{ps}, & h < c_{ps}(T_m - T_{ref}) \\ T_m, & c_{ps}(T_m - T_{ref}) \le h \le c_{ps}(T_m - T_{ref}) + l \\ T_m + \dfrac{h - l}{c_{pl}} - c_{ps}/c_{pl}(T_m - T_{ref}), & h > c_{ps}(T_m - T_{ref}) + l \end{cases} \tag{2.2}$$

For non-isothermal case, the phase change takes place as illustrated in Figure 2.4(b), the relations of the enthalpy to the temperature could be

$$h = \begin{cases} c_{ps}(T - T_{ref}), & T < T_{ms} \\ c_{ps}(T_{ms} - T_{ref}) + \dfrac{T - T_{ms}}{T_{ml} - T_{ms}} l, & T_{ms} \le T \le T_{ml} \\ c_{ps}(T_{ms} - T_{ref}) + l + c_{pl}(T - T_{ml}). & T > T_{ml} \end{cases} \quad (2.3)$$

Then the temperature could be determined by

$$T = \begin{cases} T_{ref} + h/c_{ps}, & h < c_{ps}(T_m - T_{ref}) \\ T_{ms} + \dfrac{[h - c_{ps}(T_{ms} - T_{ref})](T_{ml} - T_{ref})}{l}, & c_{ps}(T_{ms} - T_{ref}) \le h \le c_{ps}(T_{ms} - T_{ref}) + l \\ T_{ml} + \dfrac{h - l}{c_{pl}} - \dfrac{c_{ps}}{c_{pl}(T_{ms} - T_{ref})}, & h > c_{ps}(T_{ms} - T_{ref}) + l. \end{cases} \quad (2.4)$$

During melting, the thermo-physical properties will be determined by the mixture of solid and liquid as

The mixing density: $$\rho = (1 - g) \cdot \rho_s + g \cdot \rho_l. \quad (2.5)$$

The mixing thermal conductivity: $$k = (1 - g) \cdot k_s + g \cdot k_l. \quad (2.6)$$

Subscripts s and l represent solid and liquid phases, respectively. $g$ is liquid volume fraction determined by

For isothermal phase change:

$$g = \begin{cases} 0, \ T < T_m \\ \dfrac{h - c_{ps}(T_m - T_0)}{l}, T = T_m. \\ 1, \ T > T_m \end{cases} \quad (2.7)$$

For non-isothermal phase change:

$$g = \begin{cases} 0, & T < T_{ms} \\ \dfrac{(T - T_{ms})}{T_{ml} - T_{ms}}, & T_{ms} \le T \le T_{ml}. \\ 1. & T > T_{ml} \end{cases} \quad (2.7)$$

## 2.3 Finite Difference Method for Analyzing One-dimensional Phase Change Problem

The finite difference method is the basic concept for analyzing the phase change problem in fix grid method. For 1-dimensional, is given by:

$$\rho \cdot \frac{\partial h}{\partial t} = k \cdot \frac{\partial^2 T}{\partial x^2}. \tag{2.8}$$

In finite difference approach, the domain is divided into N nodes with equal segments $\Delta x = \frac{L}{N-1}$ as shown in Figure 2.5. With this arrangement, each node can be identified by:

$$x_i = (i-1) \cdot \Delta x, i = 1, 2, 3, \dots, N. \tag{2.9}$$

Nodes 1 and N are known as boundary nodes. The heat transfers in these nodes are more complicated than the internal nodes. The convection and the radiation heat exchanges are included. For the internal node, only heat conduction is considered.

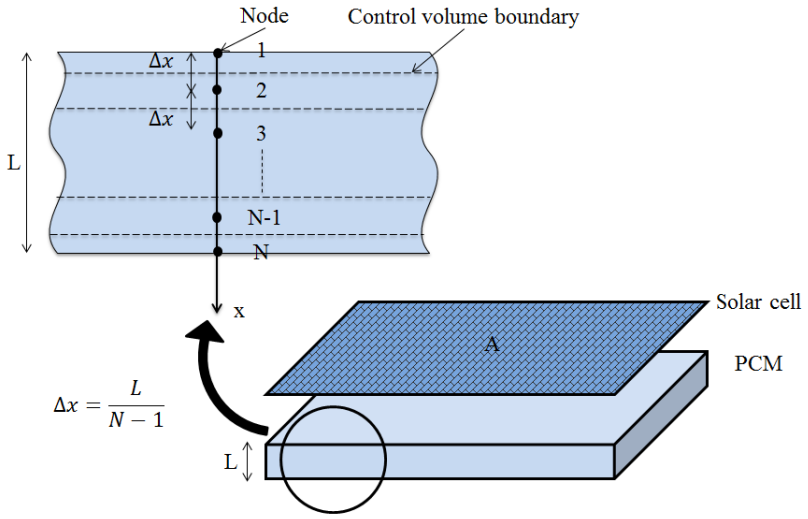


Figure 2.5 Spatial discretization step Δx of the PCM.

The basic concept of PV-PCM thermal model consists of two steps:

1. The heat transfer between different nodes at internal nodes
2. Temperature change with time steps

To obtain the solution of heat transfer problem, these two steps have to be calculated continually.

2.3.1 Heat transfer between two different nodes

At the internal node, the radiation and convection is neglected. The heat flux of heat conduction only is given by Fourier's law. It can be written in 1-dimention by:

$$\frac{dQ}{dt} = -A \cdot k \cdot \frac{dT}{dx}. \tag{2.10}$$

The division of domain into N nodes, each internal node has the same size of control volume equal to $A \cdot \Delta x$. $A$ is the area normal to the direction of heat conduction.

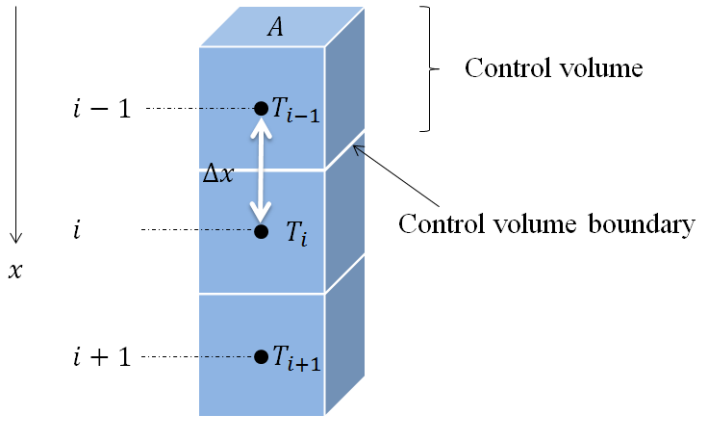


Figure 2.6 The discrete spatial divided into finite volume elements indicated by node i.

According to equation (3) and Figure 2.6, with duration time $\Delta t$, the heat conduction transfer between two neighboring nodes, i and i-1, is given by

$$\frac{\Delta Q_{i-1 \to i}}{\Delta t} = -A \cdot k \cdot \frac{T_i - T_{i-1}}{x_i - x_{i-1}}. \tag{2.11}$$

Here, $k$ is the thermal conductivity of material, $\Delta T = T_i - T_{i-1}$ is the temperature difference between nodes i and i-1, $\Delta x = x_i - x_{i-1}$ is the distance between two neighboring nodes and $\Delta t$ is time step.

2.3.2 Internal node

With the enthalpy method, the energy storage inside the control volume can be given as:

$$\rho(A \cdot \Delta x)\frac{dh}{dt}. \tag{2.12}$$

At the internal nodes, (*i*=2, 3, ...,N-1), all the energy transfers by heat conduction from neighboring nodes of node *i*, as shown in Figure 2.7 are equal to the energy stored in the control volume as

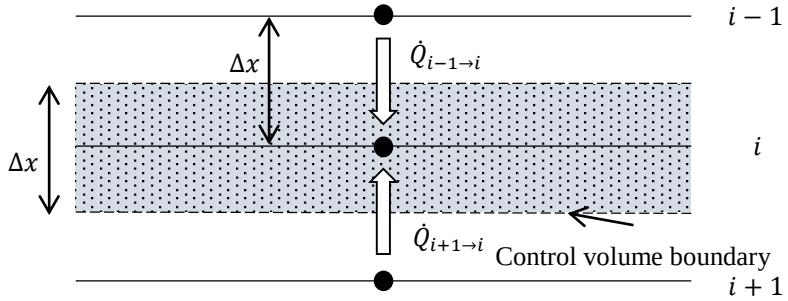


Figure 2.7 Energy from neighboring nodes conducted to the control volume of node $\boldsymbol{i}$.

$$\rho(A \cdot \Delta x)\frac{dh}{dt} = \dot{Q}_{i-1\to i} + \dot{Q}_{i+1\to i},$$

$$\rho(A\Delta x)\frac{h_i^{t+\Delta t} - h_i^t}{\Delta t} = \frac{kA}{\Delta x}\left(T_{i+1}^t - T_i^t\right) + \frac{kA}{\Delta x}\left(T_{i-1}^t - T_i^t\right),$$

Then

$$h_i^{t+\Delta t} = h_i^t + \frac{k}{\rho}\frac{\Delta t}{\Delta x^2}\left(T_{i+1}^t + T_{i-1}^t - 2T_i^t\right). \tag{2.13}$$

In cast of no phase change, the enthalpy can replace by temperature and heat capacity $h = c_P \cdot T$ then the equation (2.13) can rearrange:

$$T_i^{t+\Delta t} = \frac{k}{\rho_i \cdot c_{P_i}} \cdot \frac{\Delta t}{\Delta x^2} \cdot \left(T_{i-1}^t + T_{i+1}^t\right) + \left(1 - 2 \cdot \frac{k}{\rho_i \cdot c_{P_i}} \cdot \frac{\Delta t}{\Delta x^2}\right) \cdot T_i^t. \tag{2.14}$$

The coefficient of the temperature at previous time step $T_i^t$ is negative value; it let the calculation to be unpredictable value of the nodal temperature at the next time step $t + \Delta t$. To prevent this situation happen, the coefficient of $T_i^t$ have to be greater than or equal to zero or

$$\frac{k}{\rho_i \cdot c_{P_i}} \cdot \frac{\Delta t}{\Delta x^2} \leq \frac{1}{2}. \tag{2.15}$$

## 2.4 Boundary condition

Difference from the internal nodes, the dimensions of the superficial node at the front 1 and the back node N have only half of $\Delta x$ which is $\Delta x/2$; so the control volume of the superficial node is $A(\Delta x/2)$. The heat accumulated inside these nodes are:

$$\rho\left(A \cdot \frac{\Delta x}{2}\right)\frac{dh}{dt}.$$

### 2.4.1 Superficial node

The heat transfer at the node is more complicated than the internal node. The solar radiation from the sun, the heat convection from the module to the surrounding and the radiative exchange between the front surface of the PV to the sky are included this nodal control volume.

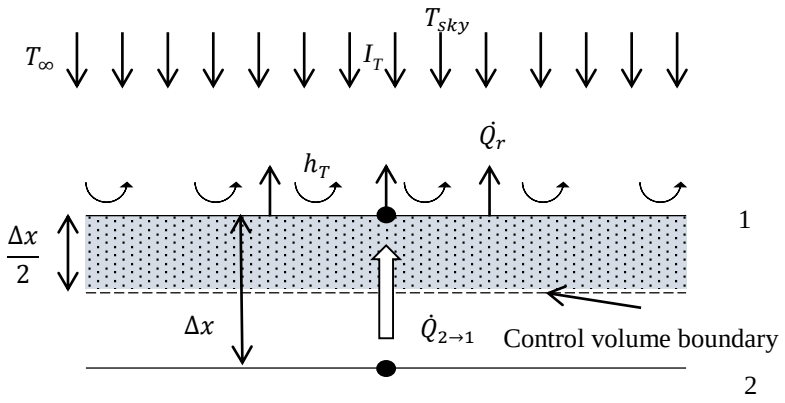


Figure 2.8 Heat transfer at top surface of module PV-PCM.

The term of the heat flux from the sun is absorbed by the solar cell module is given by

$$\dot{Q}_{sr} = I_T \cdot (\tau\alpha) \cdot A. \tag{2.16}$$

Here, $I_T$ is solar radiation, $(\tau\alpha)$ is coefficient of optical efficiency of solar cell module, and $A$ is area of absorption.

When there is temperature difference between the solar cell module surface and the ambient, there is convective heat loss from the module surface. The convective heat loss to the air surrounding is

$$\dot{Q_{cv}} = -h_T \cdot A \cdot (T_{module} - T_\infty). \tag{2.17}$$

Here, $T_\infty$ is ambient temperature and $T_{module}$ is solar cell module temperature. In simple way for numerical simulation, the thickness of solar cell is assumed to be small and temperature of solar cell module is taken to be the same value of the temperature of superficial node $T_1$. The convective heat transfer coefficient at the top surface $h_T$ is given by [27]

$$h_T = 3.0 \cdot w + 2.8. \tag{2.18}$$

That, *w* is wind speed. At Chiang Mai, Thailand the average velocity is between 0.7 to 1.7 m/s.

The radiative heat loss from top surface of the solar cell to the sky is given by

$$\dot{Q}_r = -\varepsilon \cdot \sigma \cdot A \cdot \left(T_{module}^4 - T_{sky}^4\right). \tag{2.19}$$

$\varepsilon$ is emissivity of the front surface of solar cell is given as 0.91 [27] $\sigma$ is Boltzmann constant is 5.667x10$^{-8}$. $T_{sky}$ is the sky temperature which could be commonly calculated by [5]

$$T_{sky} = 0.0552 \cdot T_\infty^{1.5}. \tag{2.20}$$

The heat conduction from the neighboring node

$$\dot{Q}_{2\to1} = -A \cdot k \cdot \frac{T_1 - T_2}{\Delta x}. \tag{2.21}$$

The heat accumulate inside control volume of the superficial node is

$$\dot{Q}_1 = \dot{Q}_{sr} + \dot{Q}_c + \dot{Q}_r + \dot{Q}_{2\to1} \tag{2.22}$$

Then,

$$\rho\left(A \cdot \frac{\Delta x}{2}\right)\frac{dh}{dt} = I_T \cdot (\tau\alpha) \cdot A - h_T \cdot A \cdot (T_1 - T_\infty) - \varepsilon \cdot \sigma \cdot A \cdot \left(T_1^4 - T_{sky}^4\right) - A \cdot k \cdot \frac{T_1 - T_2}{\Delta x}. \tag{2.23}$$

In explicit finite difference equation

$$m_1 \cdot \frac{h_1^{t+\Delta t} - h_1^t}{\Delta t} = I_T^t \cdot (\tau\alpha) \cdot A - h_T^t \cdot A \cdot (T_1^t - T_\infty^t) - \varepsilon \cdot \sigma \cdot A \cdot \left({T_1^t}^4 - {T_{sky}^t}^4\right) - k \cdot \frac{T_1^t - T_2^t}{\Delta x}. \tag{2.24}$$

Mass of control volume of superficial node $m_1 = A \cdot \frac{\Delta x}{2} \cdot \rho_1$

$$A \cdot \frac{\Delta x}{2} \cdot \rho_1 \cdot \frac{h_1^{t+\Delta t} - h_1^t}{\Delta t} = I_T^t \cdot (\tau\alpha) \cdot A - h_T^t \cdot A \cdot (T_1^t - T_\infty^t) - \varepsilon \cdot \sigma \cdot A \cdot \left({T_1^t}^4 - {T_{sky}^t}^4\right) - k \cdot \frac{T_1^t - T_2^t}{\Delta x}. \quad (2.25)$$

Separating the new enthalpy to the left side

$$h_1^{t+\Delta t} = h_1^t + 2 \cdot \frac{k}{\rho_i} \cdot \frac{\Delta t}{\Delta x} \cdot \left[I_T^t \cdot (\tau\alpha) \cdot A + h_T^t \cdot A \cdot (T_\infty^t - T_1^t) + \varepsilon \cdot \sigma \cdot A \cdot \left({T_{sky}^t}^4 - {T_1^t}^4\right)\right] + 2 \cdot \frac{k}{\rho_i} \cdot \frac{\Delta t}{\Delta x^2} \cdot (T_2^t - T_1^t). \quad (2.26)$$

It is noted worthy that the superficial node temperature of the PCM is assumed to be the same as the solar cell module temperature.

2.4.2 Bottom node

The convective heat exchange between the bottom and the surrounding is given by

$$\dot{Q}_{cv} = -h_B \cdot A \cdot (T_N - T_\infty). \quad (2.27)$$

The convective heat transfer coefficient at the bottom was followed by equation (2.18). The wind speed at the bottom was poorer than the top because it was block by ground. It is assumed that the wind speed at the back is nearly zero.

The back node is a joint between PCM and aluminum container. The aluminum has the emissivity is 0.039-0.07 [28] that is very small and the temperature at the bottom and the ambient is not so much different. The ground temperature is assumed to be equal to the ambient temperature so the radiation from the back node to the ground is neglected. The heat transfer to back note consist of only convection and heat conduction from neighboring node as shown in Figure 2.9. The energy balance is given as

$$\dot{Q}_{N-1\to N} + \dot{Q}_{cv} = \rho\left(A\frac{\Delta x}{2}\right)\frac{\partial h_N}{\partial t},$$

$$\frac{kA}{\Delta x}(T_{N-1}^t - T_N^t) + h_B \cdot A \cdot (T_\infty - T_N) = \rho\left(A\frac{\Delta x}{2}\right)\frac{h_N^{t+\Delta t} - h_N^t}{\Delta t},$$

Then

$$h_N^{t+\Delta t} = h_N^t + 2\frac{k}{\rho}\frac{\Delta t}{\Delta x^2}\,(T_{N-1}^t - T_N^t) + 2\frac{k}{\rho}\frac{\Delta t}{\Delta x^2}h_B(T_\infty - T_N). \qquad (2.28)$$

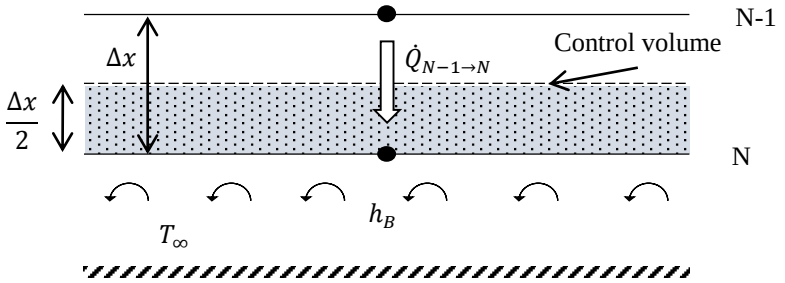


Figure 2.9 Heat transfer at the bottom.

## 2.5 Initial Conditions

At initial time, for validation with experimental data, the calculation will choose the temperature all node of PCM is assumed to be equal to the initial temperature from the experiments (Top, Middle and Bottom) and other layer will obtain by fitting curve of temperature and distance $(T, x)$ as shown in Figure 2.10; the enthalpy reference $h\_ref$ will be chose to be zeros at the temperature is equal to zero degree Celsius.

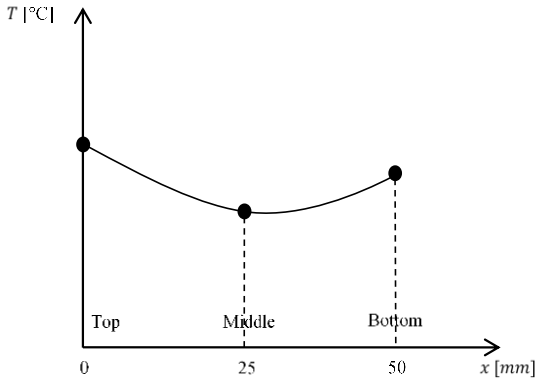


Figure 2.10 The initial temperature and the position of PCM.

## 2.6 Algorithm with MATLAB Programming

The numerical solution has been done by enthalpy method and effective heat capacity method as in Table 2.2. Some program tools such as MATLAB, ESP-r, EnergyPlus and TRNSYS is used.

In this study, the simulation code was developed in MATLAB Programming. One-dimensional energy equation was written. The spatial discretization and time step were chosen $\Delta x = 1\ mm$ and $\Delta t = 1\ s$, respectively.

Table 2.2 Review numerical method and programming tool for solving phase change problem.

| Computing Program | Numerical method | Form | Computational methods | References |
|---|---|---|---|---|
| ESP-r | Effective heat capacity | Finite volume | Explicit | [24] |
| MATLAB | Enthalpy method | Finite volume | Crank-Nicholson | [23] |
| EnergyPlus | Enthalpy method | Finite difference | Implicit | [29] |
| TRNSYS Type 260 | Effective heat capacity | Finite difference | Explicit | [25] |

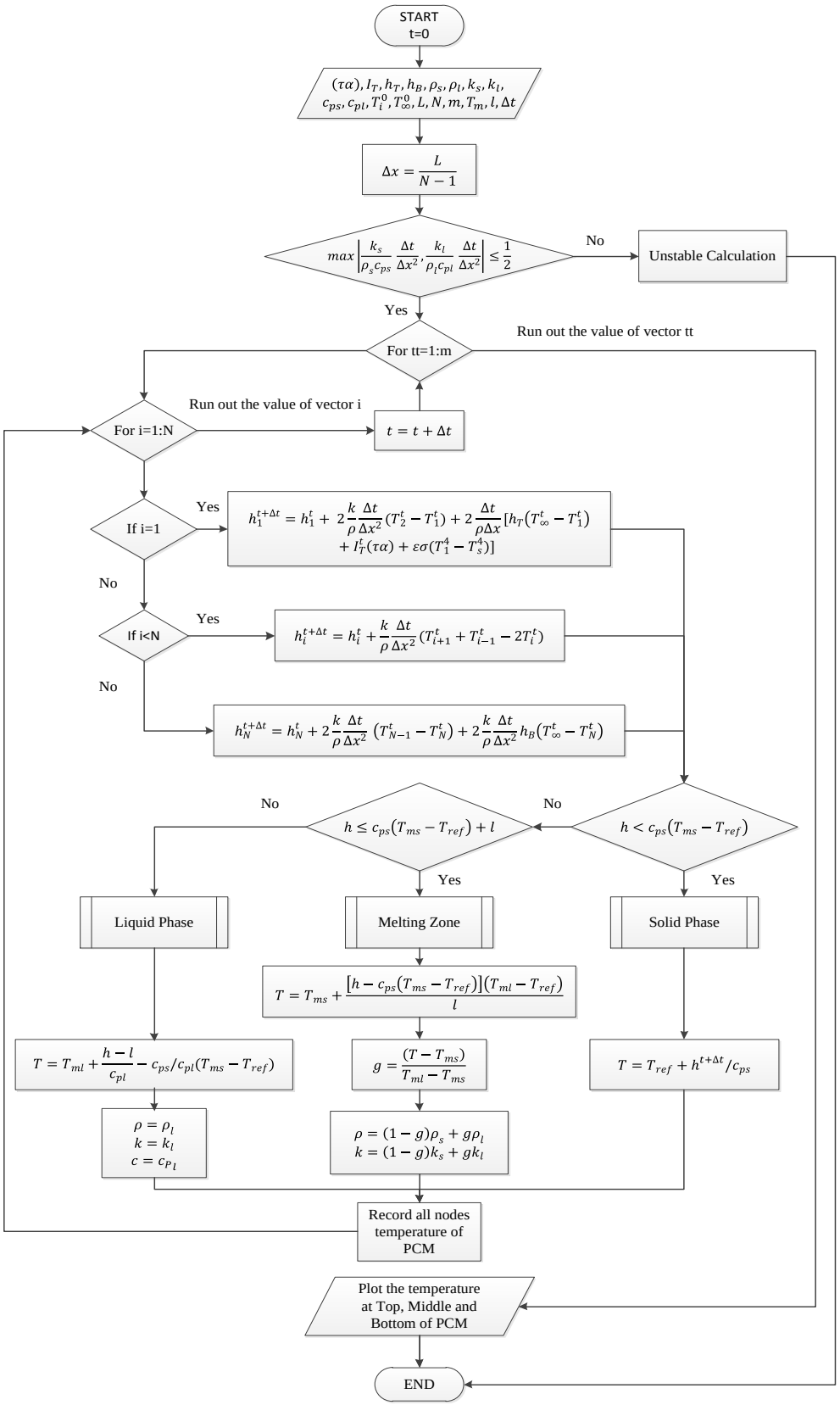


Figure 2.11 Flowchart of enthalpy method for solving heat transfer in PCM.

## 2.7 PCM for Simulation

Four types of commercial RUBITHERM® RT PCMs are used in simulation as given in the Table 2.3. RT42 PCM is used in both experiment and simulation, the verification is required to make sure that our model is good for predicting the temperature of PCM and solar cell.

In the simulation, the enthalpy is used to predict the temperature of PCM. In this case the latent heat needs to separate from the heat storage capacity as give in the Table 2.3. The heat storage of RT35, RT42, RT47 and RT55 are 160, 174, 170 and 172 kJ/kg which the storage temperature range of 26-41, 35-50, 39-54 and 48-63 °C, respectively. As given in Figure 2.12, the latent heat of melting can be sum up partial enthalpy during the melting. The latent heat of melting of RT35, RT42, RT47 and RT55 is 147, 144, 136, 132 kJ/kg, respectively.

Table 2.3 Thermo-physical properties of PCMs [30].

| Type | RT35 | RT42 | RT47 | RT55 |
|---|---|---|---|---|
| Melting temperature range [°C] | 29-36 | 38-43 | 41-48 | 51-57 |
| Solidification temperature range [°C] | 36-31 | 43-37 | 48-41 | 56-57 |
| Heat storage capacity [kJ/kg] | 160 | 174 | 170 | 172 |
| Specific heat [kJ/kg-K] | 2 | 2 | 2 | 2 |
| Density in solid [kg/$m^3$] | 860 | 880 | 880 | 880 |
| Density in liquid [kg/$m^3$] | 770 | 760 | 770 | 770 |
| Thermal conductivity [W/m-K] | 0.2 | 0.2 | 0.2 | 0.2 |

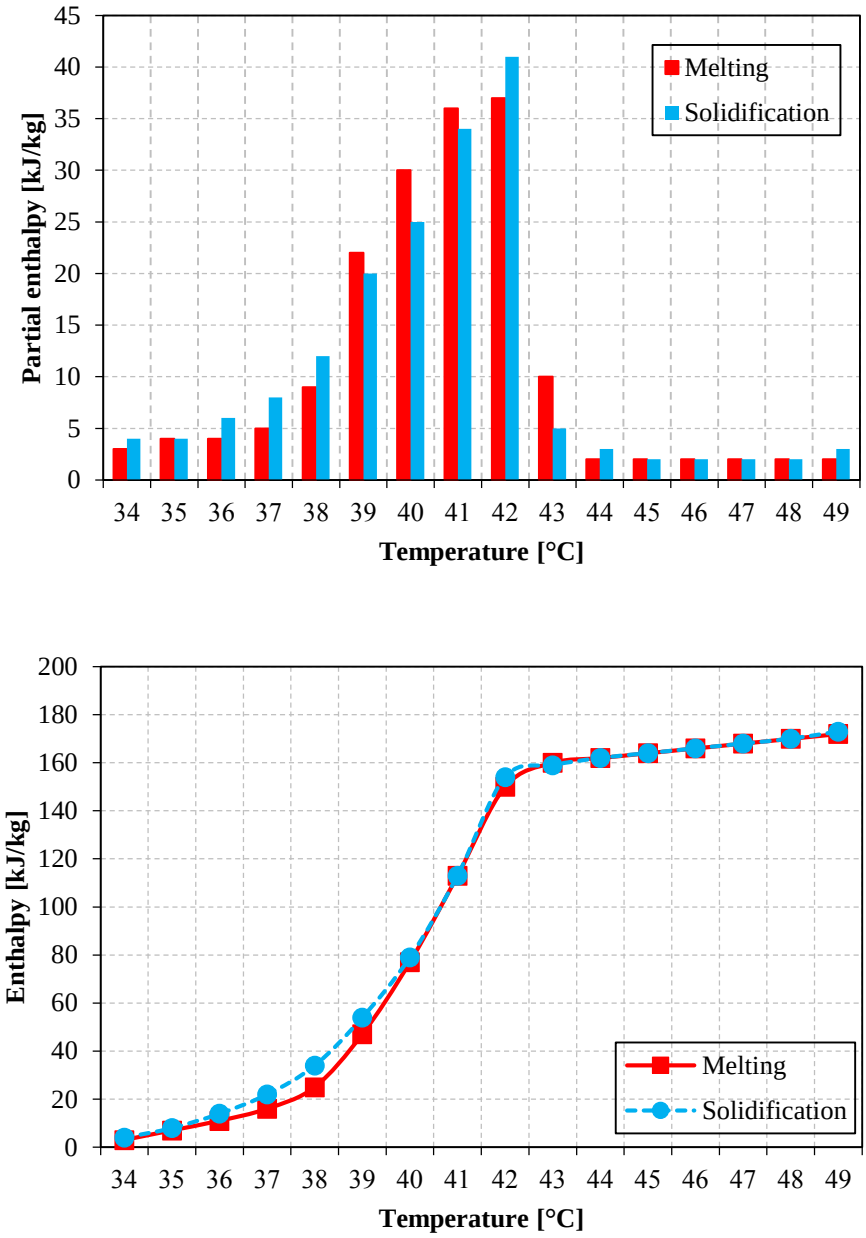


Figure 2.12 Enthalpy and Temperature relation base on spec from manufacturer RUBITHERM® RT42.

# Chapter 3
# Experimental Setup

This chapter provides an experimental description and some equipment are used. The procedure of testing and function of instrument are described in this section.

## 3.1 Experimental Setup

Two identical solar cells were tested in this experiment. One unit had RT42 PCM at the back and named PV-PCM while the other one without PCM was used as a reference and named PV-R. The PV-PCM, PV-R modules were tested outdoor, facing south with 10° inclination angle in Chiang Mai, Thailand. A set of T-type thermocouples (9 points) was connected at the back of each module. For PV-PCM system, 6 points more were added to measure at the middle and the bottom layers of the PCM with a data-logger S220-T8 as shown in Figure 3.1. Another thermocouple was used for measuring the ambient temperature $T_a$. The solar radiation could be recorded by a CMP3 Pyranometer with a data-logger, EXPERT EX9018P.

Table 3.1 Electrical characteristics of EMS250-156 at Standard Testing.

| Item | Value | Unit |
|---|---|---|
| Maximum power (Pm) | 250 | Wp |
| Maximum power voltage (Vmp) | 35.5 | V |
| Maximum power current (Imp) | 7.07 | A |
| Open circuit voltage (Voc) | 43.51 | V |
| Short circuit current (Isc) | 7.91 | A |

Measurement of electrical power from the solar cell module could be performed by a multi-meter, UNI-T UT204. Two 150 W lamps (13117 150W GX5.3 17V 1CT) as shown in Figure 3.1 were used as the external load of the solar cell module. The electrical power output from the module was calculated by

$$P_e = V \times I \tag{3.1}$$

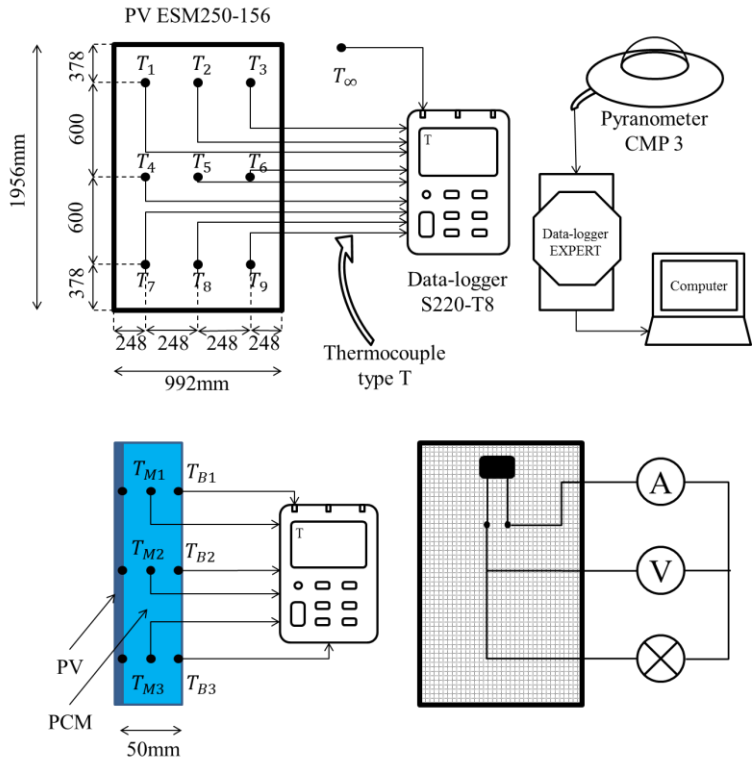


Figure 3.1 Schematic diagram of experimental setup.

## 3.2 Experimental Procedure

The experiment begins to operate under these conditions:

- The experiment will be collected data from 9:30am to 15:30pm.
- The experiment will operate in condition of clear sky day and partly cloudy day.
- The module temperatures will collection in every minute by thermocouple type-T and data-logger S220-T8.
- The value of solar radiation will obtain by sensor pyranometer (Kipp and Zonen CMP3) connect with data-logger EXPERT EX9018P. The collection is record in every minute.
- Measure electrical current and voltage of both PV-PCM and PV-R by multi-meter every 5 minutes.

Figure 3.2 Module solar cell PV-R (left) and PV-PCM (right).

Figure 3.3 RT42 PCM.

3.2.1 Measurement

Many instruments were used during the testing such as: pyranometer, data-logger, thermocouple and multi-meter were illustrated in Figure 3.4. The accuracy of all equipment was given in Table 3.2.

a. Pyranometer (Kipp and Zonen CMP3).


b. Data-logger S220-T8.

c. Thermocouple type-T.


d. Data-logger Ex9018.

e. Multi-meter UNI-T UT201.

Figure 3.4 Measuring instrumentation.

Table 3.2 Accuracy of the experimental equipment.

| Sensor | Characteristics | Accuracy |
|---|---|---|
| Data-logger S220-T8 and thermocouple type T | Measure the temperature of solar module and ambient temperature. Range: −200 to 350 °C | ±0.7°C |
| Data-logger Expert EX9018P and Pyranometer CMP3 | Measure solar radiation. Range: 0 to 2000 W/m² | ±3.5% |
| Multi-meter UNI-UT204 | Measure DC Voltage. Range: 4 to 400V | ±0.8% |
| Multi-meter UNI-UT204 | Measure DC Current. Range: 0 to 40A | ±2% |

### 3.3 Problem During the Experiment

The attached PCM at the back of solar cell, the bending of the module solar cell is occurred by the pressure of PCM liquid and high inclination. The latitude at Chiang Mai is 18° north but in this experiment the solar cell was installed with inclination 10° facing to the south.

### 3.4 Expected Results

The module temperature of the solar cell with PCM will be reduced and more electrical power will obtain. The absorbed heat during the daytime of PCM will release to surrounding during the nighttime. The temperature from the experiment will be used to verify with the simulation model of PV-PCM system. With a goodness of simulation model using the enthalpy method, the appropriate thickness of the commercial PCMs will be determined. Correlation of the optimum voltage and optimum current with the effect of solar radiation and the module temperature will indicate in the next chapter.

# Chapter 4
# Results and Discussion

This chapter describes about the potential of PCM for reducing the module solar cell temperature and more electrical generation. The validating temperature of the simulation model and the experimental result was detailed in this section. With this model, the appropriate thickness of PCMs for attaching with PV was found.

## 4.1 Temperature of Solar Cell Module with PCM

Figure 4.1 shows the surface temperatures of the tested solar cell with and without 50 mm RT42 PCM under a clear sky and cloudy condition. During the cloudy condition as shown in Figure 4.1(a), it could be seen that the temperature of the module with PCM increased gradually and the module temperature could be controlled to be less than that without the PCM. The maximum temperature difference was around 11.4 °C. Around noon, the time difference of PV-PCM and PV-R is about 8 °C. With clear sky day in the hot season in April, the module PV-R temperature reached the maximum temperature of 66.6 °C and the module PV-PCM reached the maximum temperature of 59.3 °C. Even in the cloudy condition, the solar cell module temperature was still lower than solar cell without PCM as detailed in Figure 4.1(b) and the maximum temperature difference was 13.1 °C in that day. The maximum PV-R module temperature is 60 °C while the PV-PCM module temperature is 50 °C.

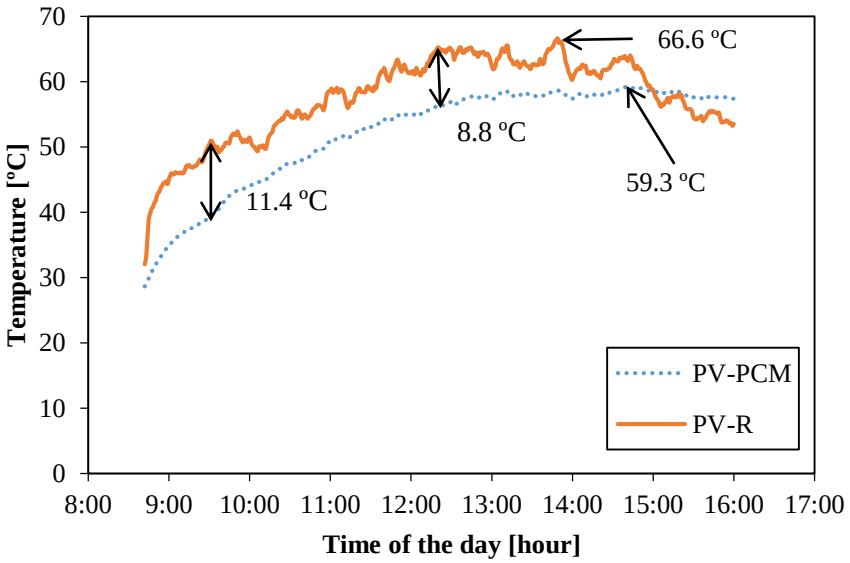


a. Clear sky day (April 27, 2015).

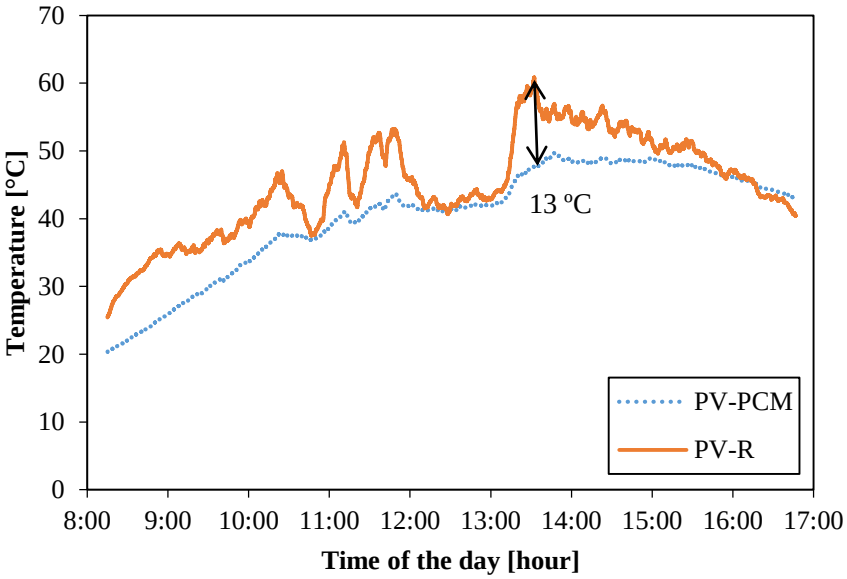


b. Partly cloudy day (March 2, 2016).

Figure 4.1 Comparison of module temperature of PC with and without RT42 PCM of the experiment.

## 4.2 Temperature PCM in 2 Consecutive Days

Figure 4.2 demonstrates about the temperature of PCM in 2 consecutive days testing. The solar radiations of those days were nearly the same value and the maximum radiation was 870 W/m$^2$. At the beginning of the first experimental day, the initial temperature of the all PCM was lower than the ambient temperature. The temperature of PCM at middle was lower than the temperature at top and bottom. After the PV-PCM system operated under the sun, the temperatures of the PCM started to increase sharply with the solar radiation rose sharply. At noon, solar radiation peaked at 870 W/m$^2$ but the temperature of PCM at top layer was still increasing until 13:00. From 13:00to 15:00 temperature of PCM at top was nearly constant at 50 °C. The temperature of PCM at the top was higher than the middle and the bottom cause by the PCM has the small thermal conductivity was reported in Table 2.3. The temperature of PCM at the top was still higher than middle and bottom until the solar radiation was gradually absent. And during the nighttime, the PCM was cooled by the surrounding and total PCM could be in solid phase with the temperature close to the ambient temperature before starting on the next day.

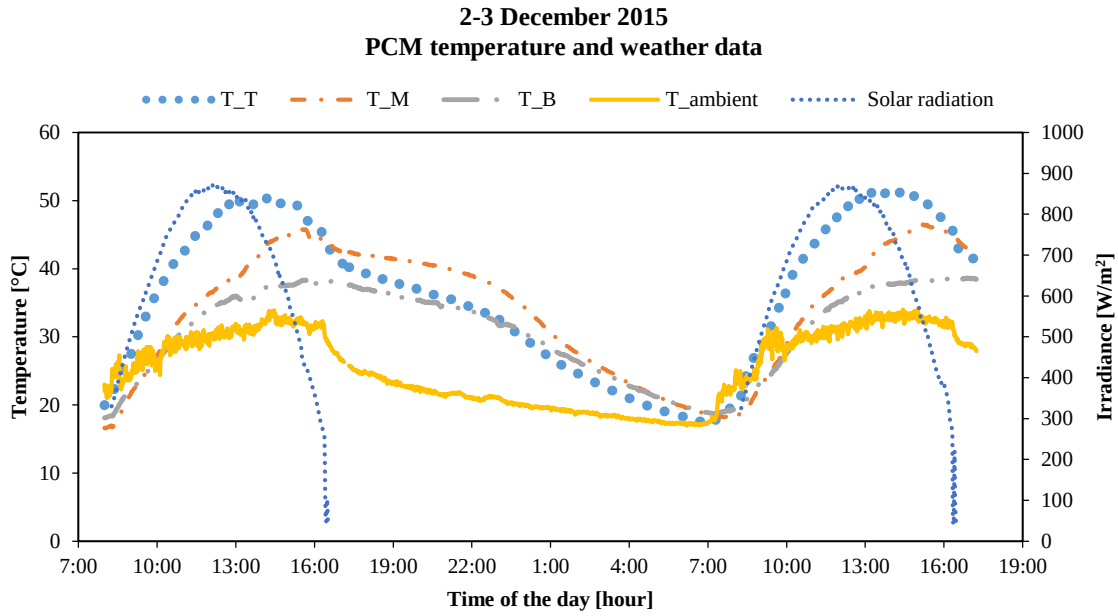


Figure 4.2 Temperature profiles of PCM top, PCM middle, PCM bottom, ambient temperature and irradiance, in Chiang Mai, December 2-3, 2015 (experiment).

## 4.3 Simulation Validation

To verify the model to be good for predicting the thickness of different type of PCMs with PV, 6 days of experiment was selected, 3 days in clear sky condition and other 3 days in partly cloudy condition. The weather data were given in Figure 4.3.

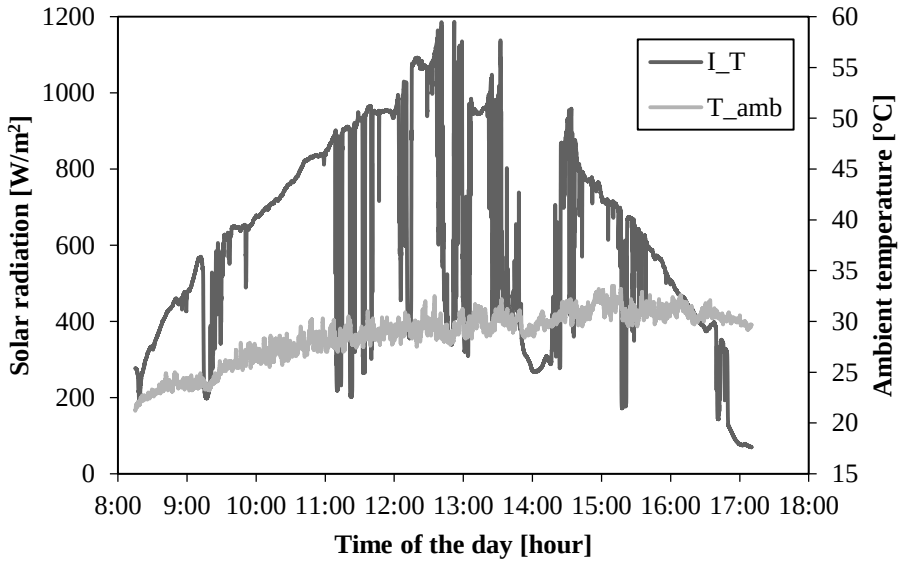


a. Partly cloudy day (February 29, 2016).

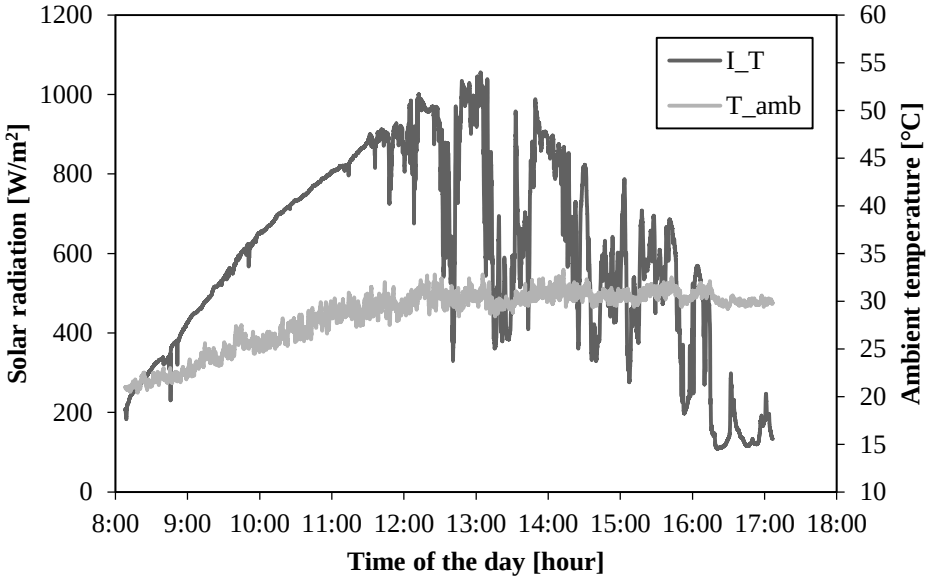


b. Partly cloudy day (March 1, 2016).

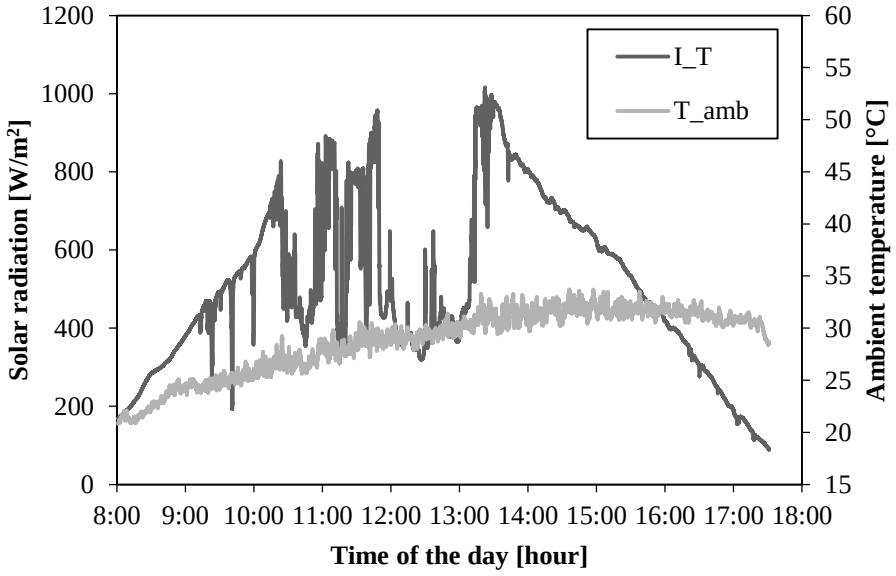


c. Partly cloudy day (March 2, 2016).

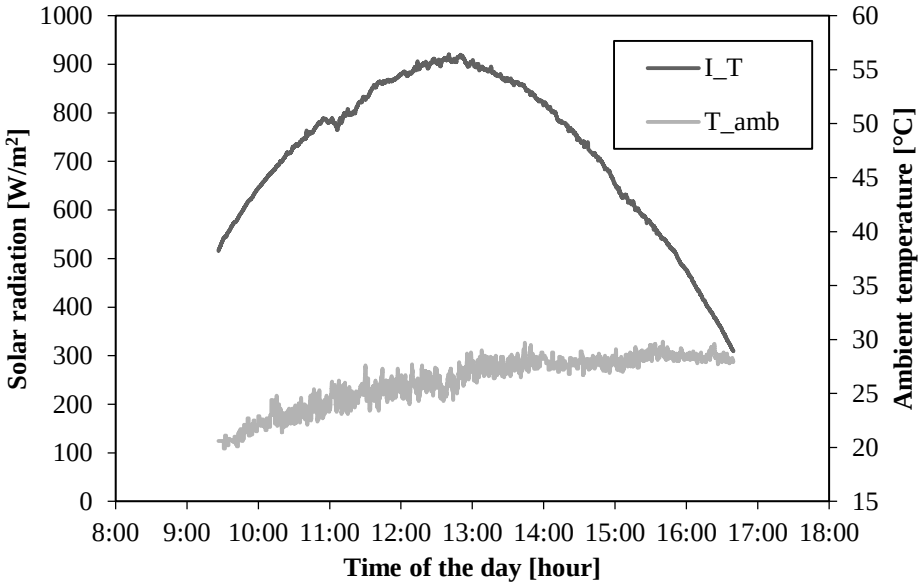


d. Clear sky day (January 30, 2016).

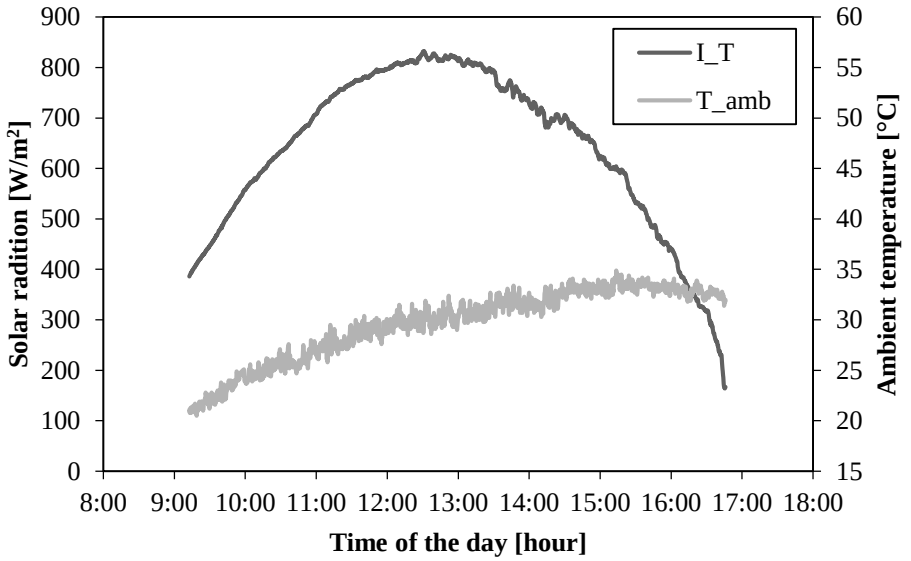


e. Clear sky day (February 15, 2016).

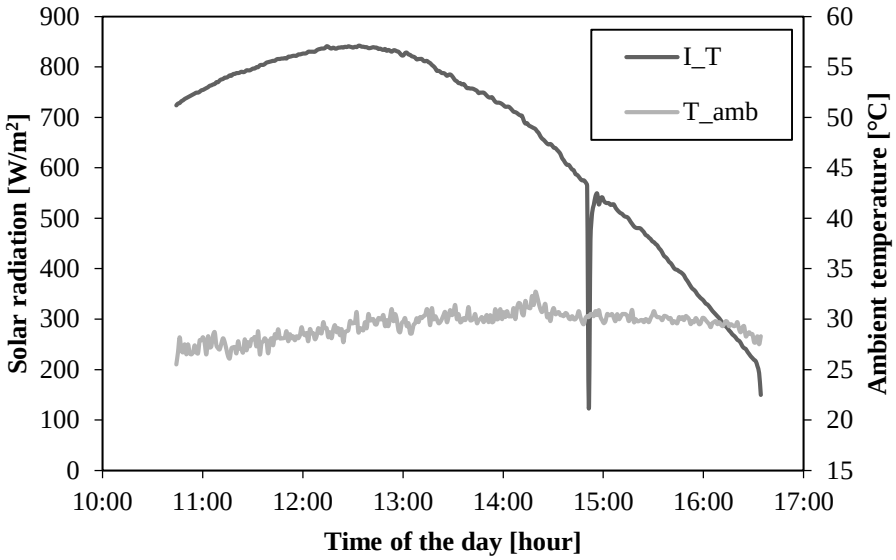


f. Clear sky day (December 15, 2015).

Figure 4.3 The weather data collect at Chiang Mai, Thailand.

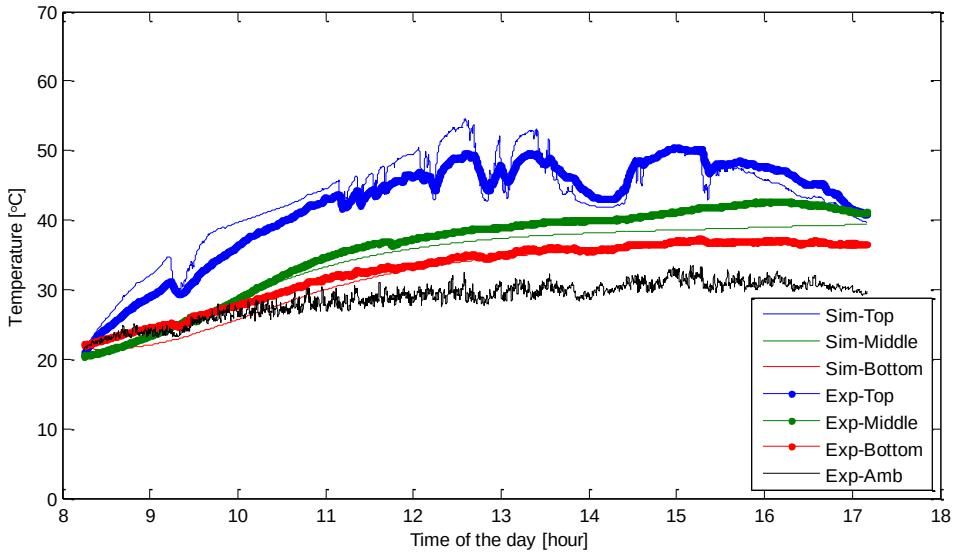


a. (February 29, 2016)

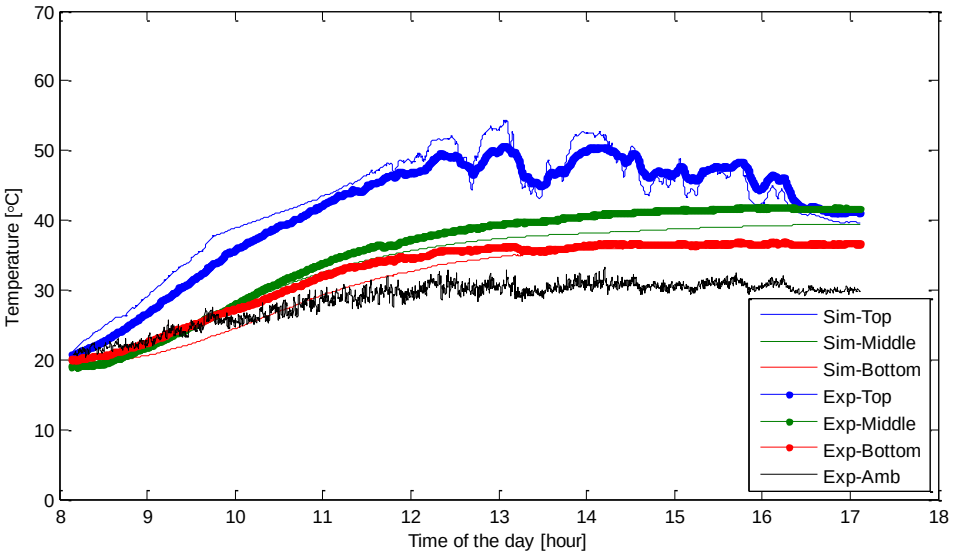


b. (March 1, 2016)

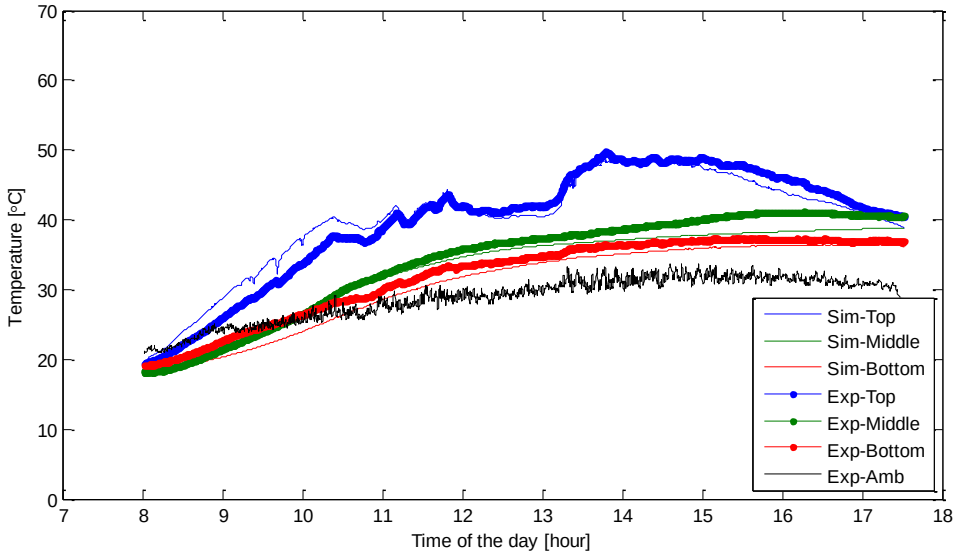


c. (March 2, 2016)

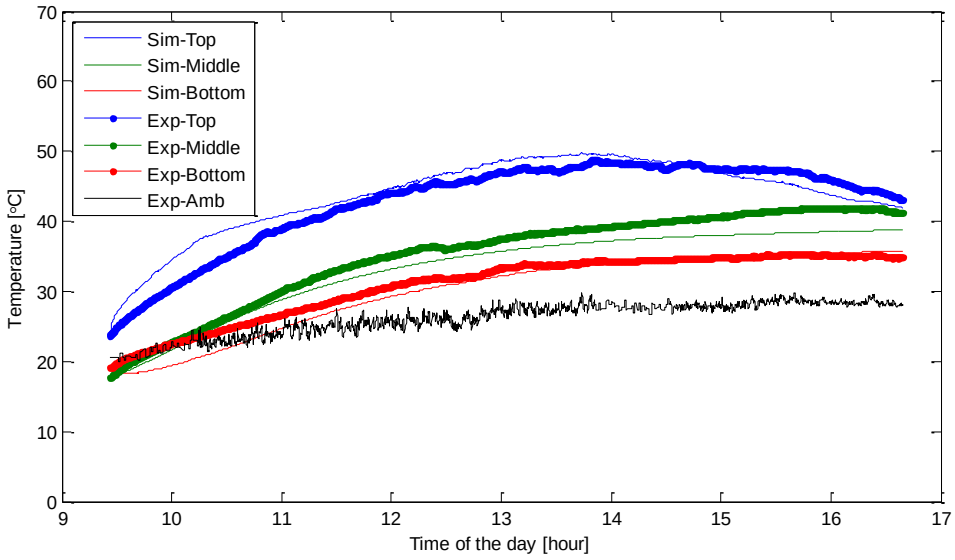


d. (January 30, 2016)

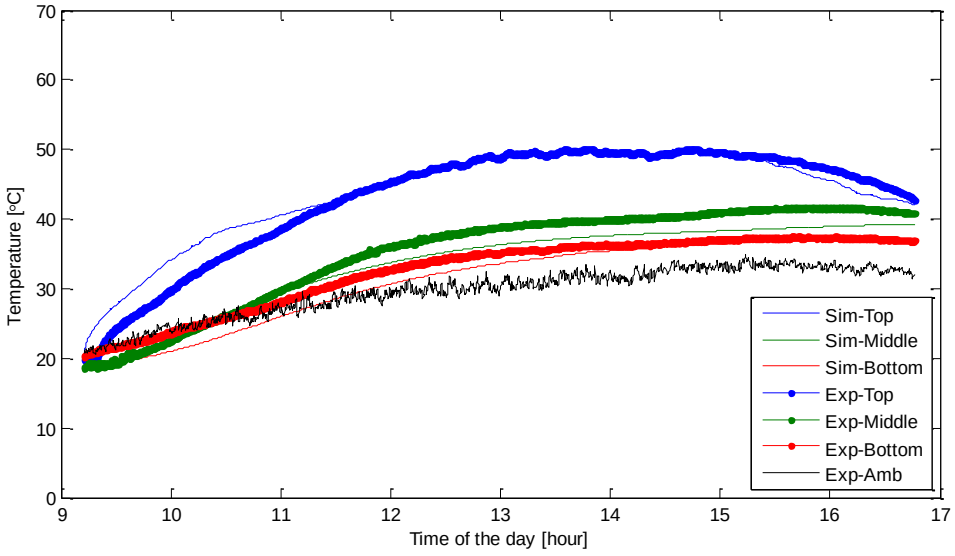


e. (February 15, 2016)

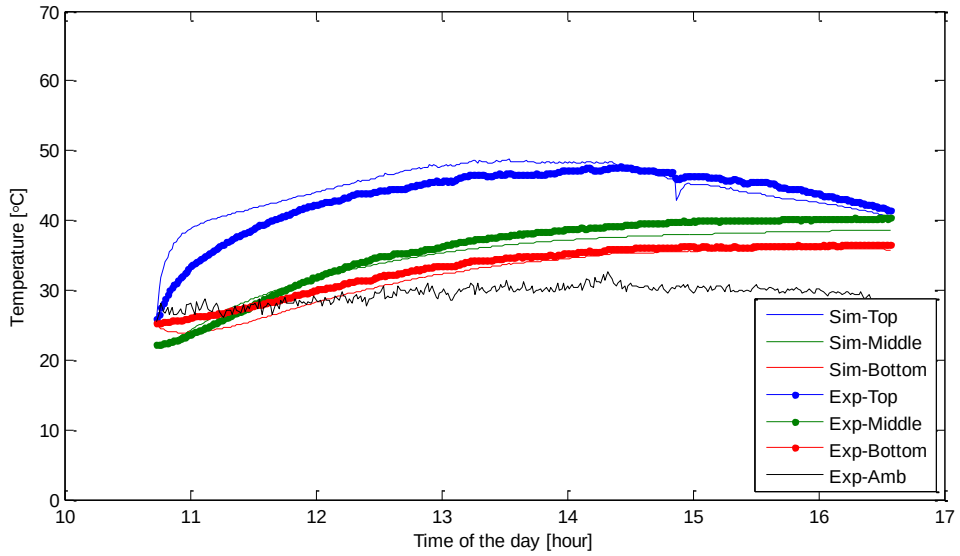


ง. (December 15, 2016)

Figure 4.4 The validation of the model with the experimental data at Chiang Mai.

The 3 days with partly cloudy and 3 days with clear sky of experimental data were used to verify our model as shown in Figure 4.4. Even in the cloudy and clear sky day, the model was good to predict the whole temperature of the PCM. Table 4.1 show the deviated $\pm 10\%$ of simulation data with experimental data. The 6 days of the simulation results deviated within $\pm 10\%$ of experimental data were over than 90%. The experimental and simulation temperature of PCM in 6 days were shown in Figure 4.5.

Table 4.1 Deviated $\pm 10\%$ of the simulation result with the experimental data.

| Date | Sky condition | Deviated $\pm 10\%$ error with experimental data |
|---|---|---|
| February 29, 2016 | Partly cloudy | 96.5380% |
| March 1, 2016 | Partly cloudy | 95.1550% |
| March 2, 2016 | Partly cloudy | 93.7992% |
| January 30, 2016 | Clear sky | 90.4476% |
| February 15, 2016 | Clear sky | 90.2609% |
| December 15, 2015 | Clear sky | 96.6762% |
| Average: | | 93.8129% |

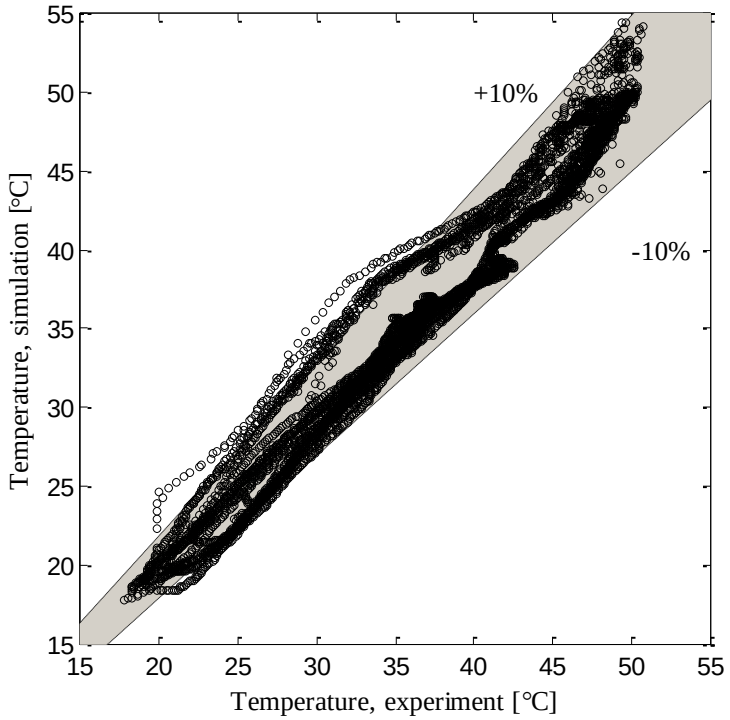


Figure 4.5 The validation of PCM temperature between experiment and simulation in 6 days.

## 4.4 Appropriate thickness of PCMs

The amount of PCM make the system PV-PCM is heavy and the appropriate PCMs are defined that our PCM can reduce the PV module temperature to be lower than normal PV. The high solar radiation and the high ambient temperature were selected for simulation to find out the thickness of PCM. In this section 4 types of commercial PCMs was chosen: RT35, RT42, RT47 and RT55 and the thermo-physical properties were given in Table 2.3. The weather data on April 27, 2015 was used for simulating to find the appropriate thickness of each PCM due to the high solar radiation and temperature as given in Figure 4.6.

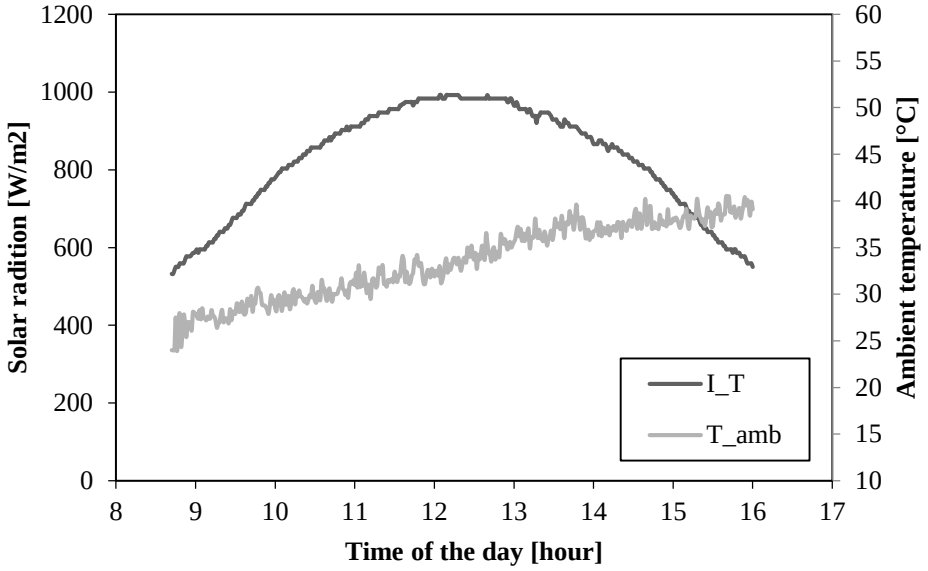


Figure 4.6 Weather data on April 27, 2015.

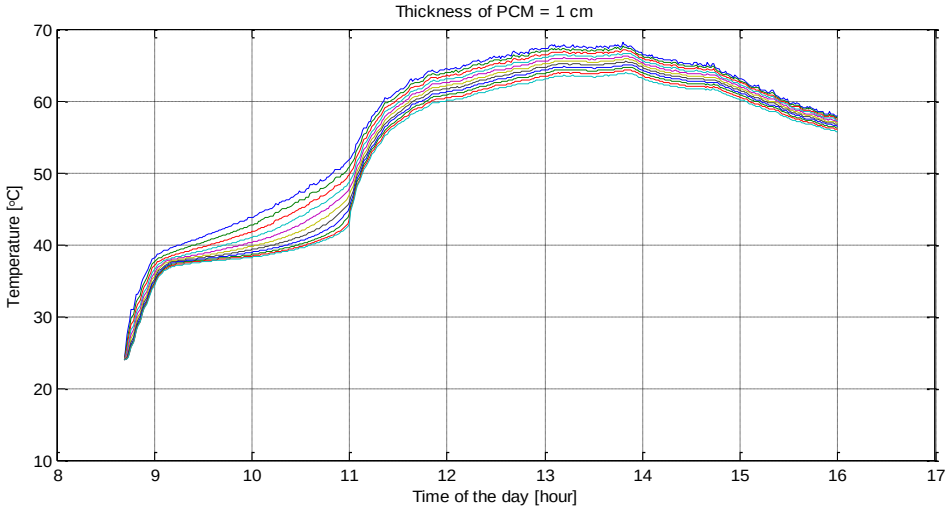


a. Thickness of 10 mm

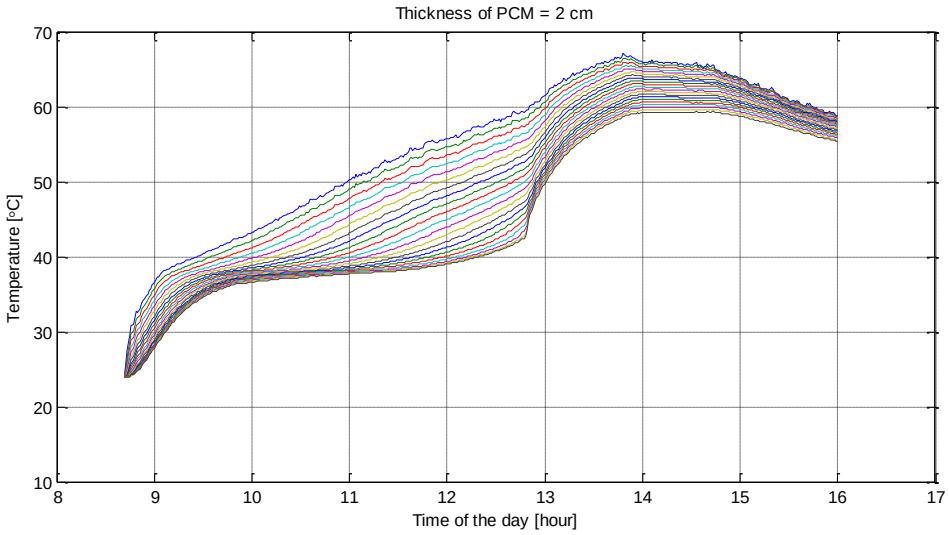


b. Thickness of 20 mm

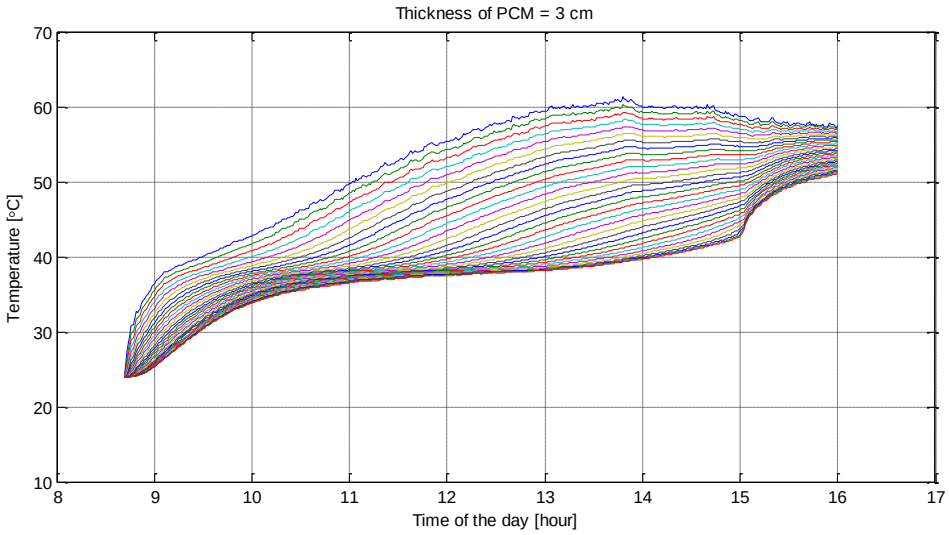


c. Thickness of 30 mm

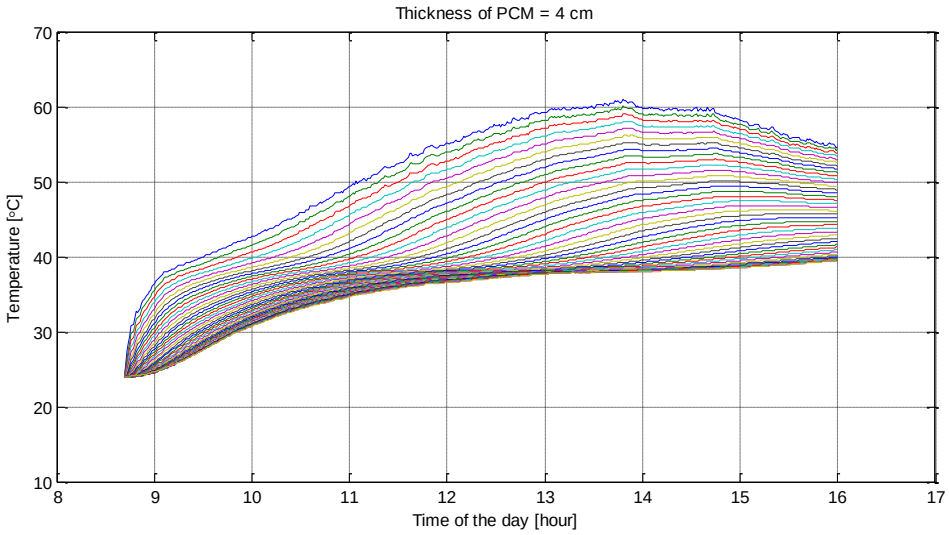


d. Thickness of 40 mm

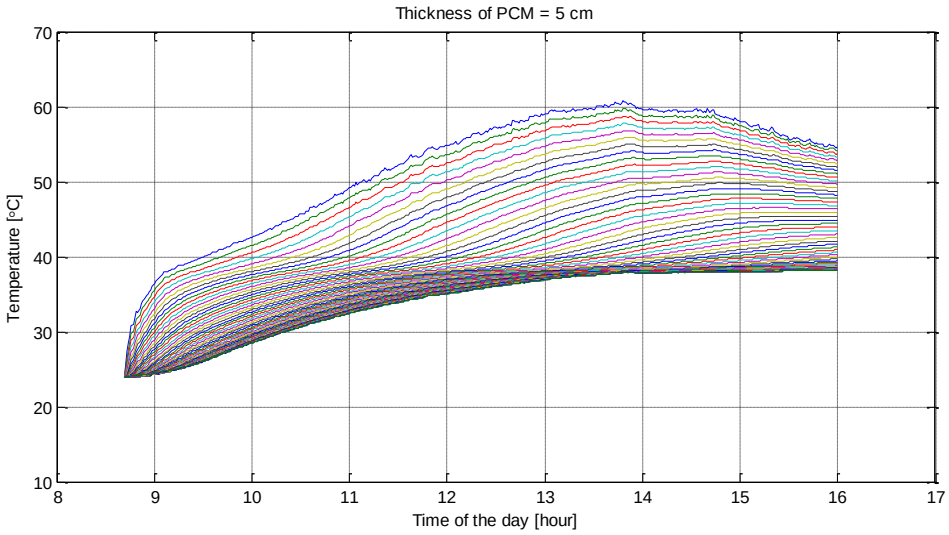


e. Thickness of 50 mm

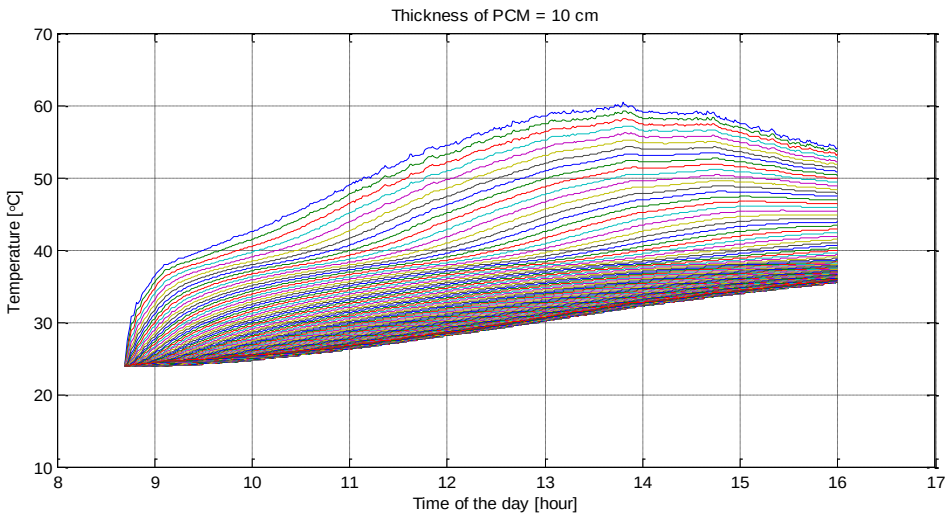


f. thickness of 100 mm

Figure 4.7 The simulation with various thicknesses of RT42 (simulation).

Figure 4.7 showed the simulation the whole temperature of RT42 PCM in various thicknesses. The comparing surface temperature of each thickness was illustrated in Figure 4.8(a). With a thickness of 10 mm in solid blue, at the 11:00 the surface temperature was shooting up to till the maximum temperature of 67 °C due to the whole PCM was complete liquid as shown in Figure 4.7(a). With a thickness 20 mm, the shooting temperature was delay in 2 hours in Figure 4.7(b). With the thickness thicker than or equal to 40 mm, the whole PCM was not completed melting. Figure 4.8(b) showed the surface temperature of RT35. With the thickness 10 mm, the RT35 started shooting since 10:00. With the thickness thicker than 50 mm, the shooting was not happen which mean that the thickness of 50 mm is enough for RT35. In conclusion, with the simulation we found that the appropriate thickness of RT35, RT42, RT47 and RT55 was 50, 40, 30 and 20 mm.

The comparing the surface temperature of each PCM with appropriate thickness was detailed in Figure 4.9. RT55 was higher than other 3 PCMs cause by the melting temperature range is high. At the begging of the simulation, the surface temperature of RT35 was lower than others. After 11:00, the surface temperature of RT35 and RT42 were closed together while the RT47 was a little bit higher. So, RT42 was the best choice to couple with solar cell even the RT35 showed the temperature lower than but thickness was thicker than RT42.

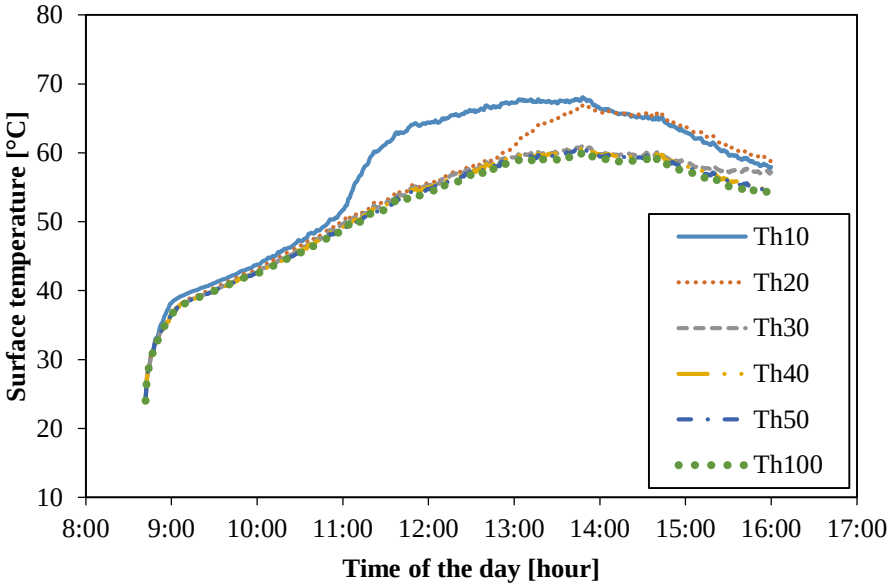
Surface temperature [°C]
80
70
60
50
40
30
20
10
8:00
9:00
10:00
11:00
12:00
13:00
14:00
15:00
16:00
17:00
Time of the day [hour]
Th10
Th20
Th30
Th40
Th50
Th100

a. RT42

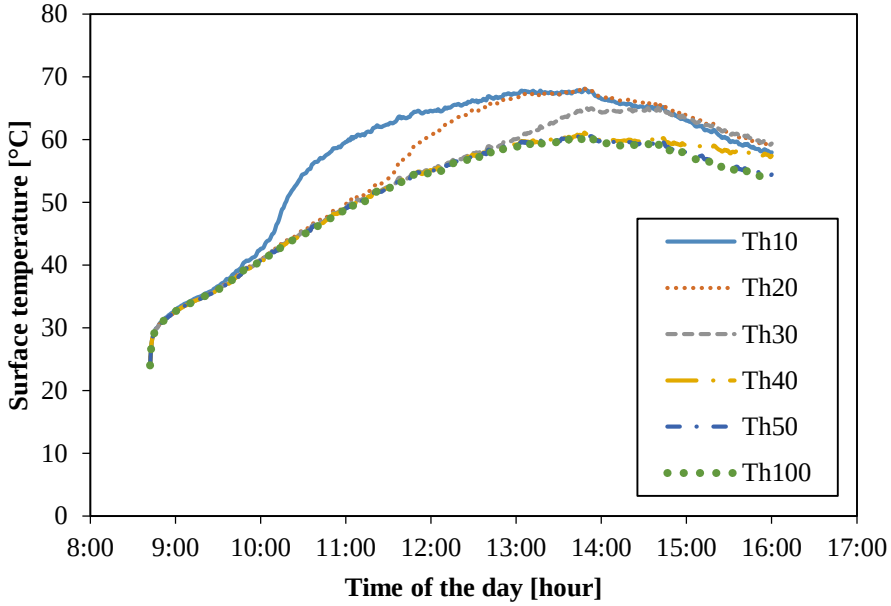
Surface temperature [°C]
80
70
60
50
40
30
20
10
0
8:00
9:00
10:00
11:00
12:00
13:00
14:00
15:00
16:00
17:00
Time of the day [hour]
Th10
Th20
Th30
Th40
Th50
Th100

b. RT35

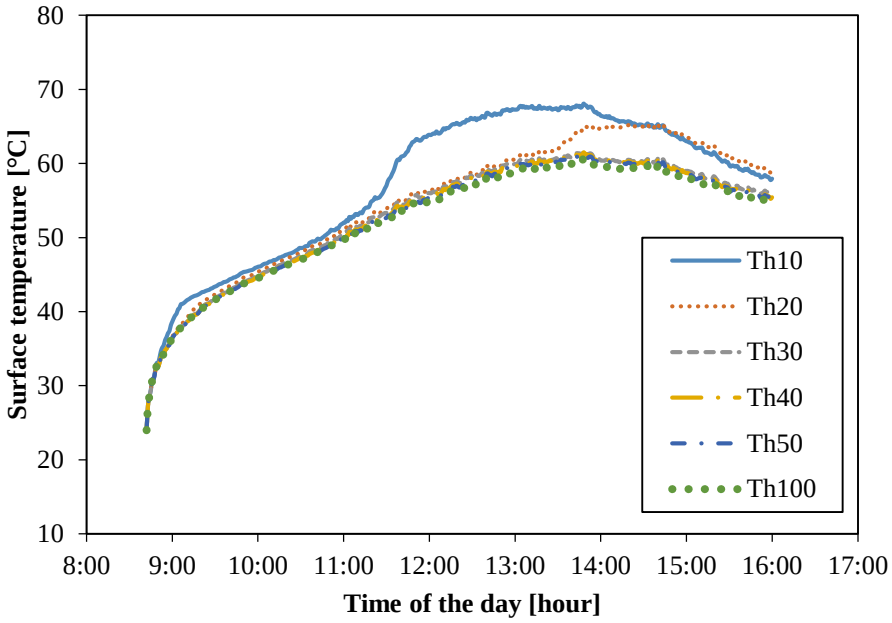


c. RT47

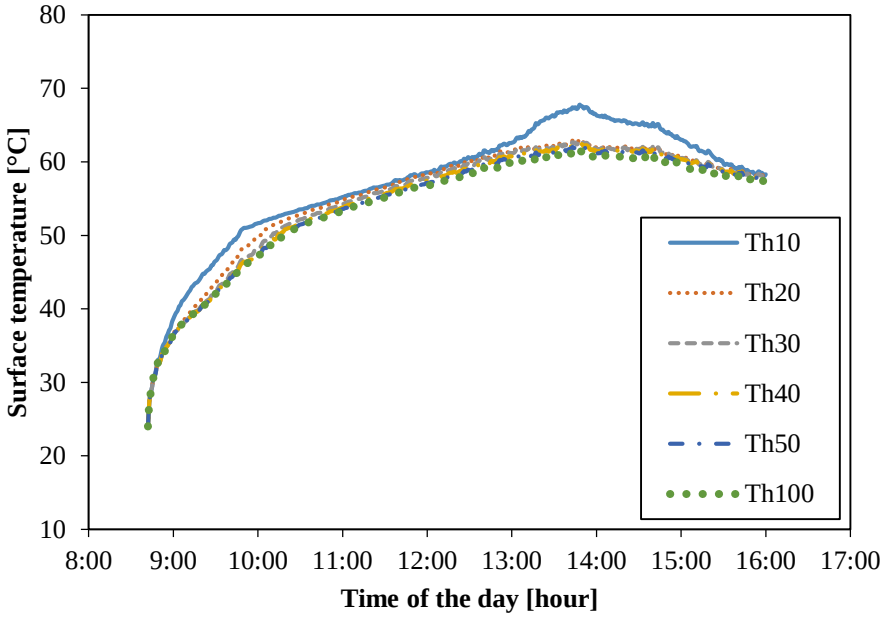


d. TR55

Figure 4.8 Surface temperature at various thicknesses of RT PCM (Simulation).

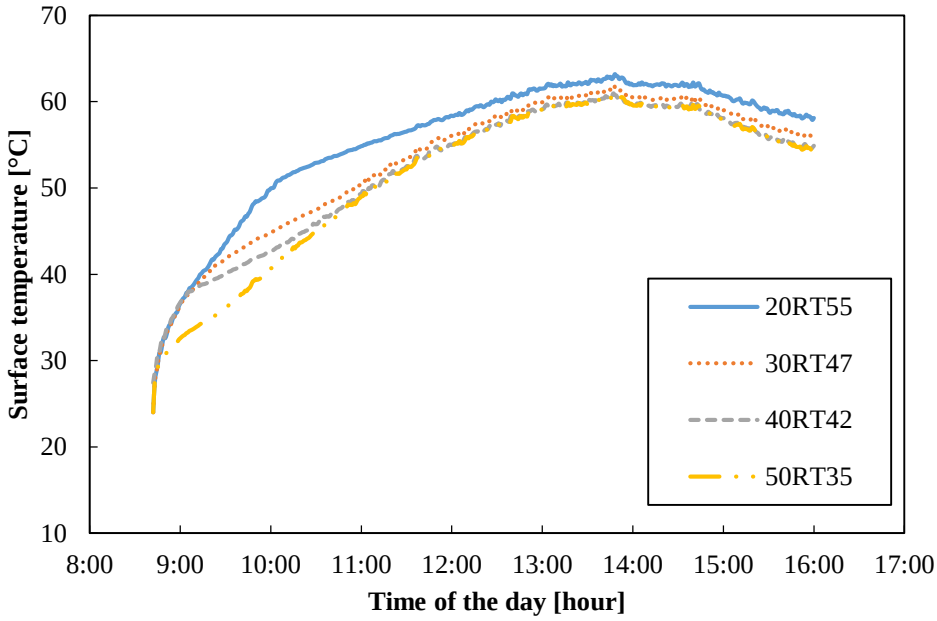


Figure 4.9 Comparison of the surface temperatures with the PCMs with different melting points (simulation).

## 4.5 Power Generation

The electrical power was gain with reducing the solar cell module temperature.

Figure 4.10 presents the generated electrical power from the solar cell modules with and without 50 mm RT42 PCM under clear sky condition (data from December 3, 2015) and presents under cloudy condition (data from December 1, 2015). The electrical power was measured in every 5 minutes from 9:30 to 15:30.

At the clear sky day as shown in Figure 4.10(a), the solar cell module PV-PCM and PV-R got highest power generation of 167 W and 147 W at noon, respectively. Within duration 6 hour and the solar radiation maximum and minimum of 867 and 468 W/m$^2$, the solar cell PV-PCM and PV-R could generate electrical energy about 0.707 and 0.642 kWh, respectively. With the RT42 PCM, the efficiency of solar cell could increase 10% in average.

Figure 4.10(b) show the electrical power of solar cell and the solar radiation on partly cloudy day. From 9:30 to 12:40, the solar radiation increase gradually to the maximum value of 933 W/m$^2$ after that the solar radiation was fluctuated by the cloud and some time it was lower than 100 W/m$^2$. At this day, the maximum power output of PV-PCM and PV-R is 207 and 183 W at the maximum solar radiation. In this day, the solar cell PV-PCM generated the electrical energy of 0.736 kW while the PV-R generated only 0.666 kW so 10 % of energy was increased by the module with PCM.

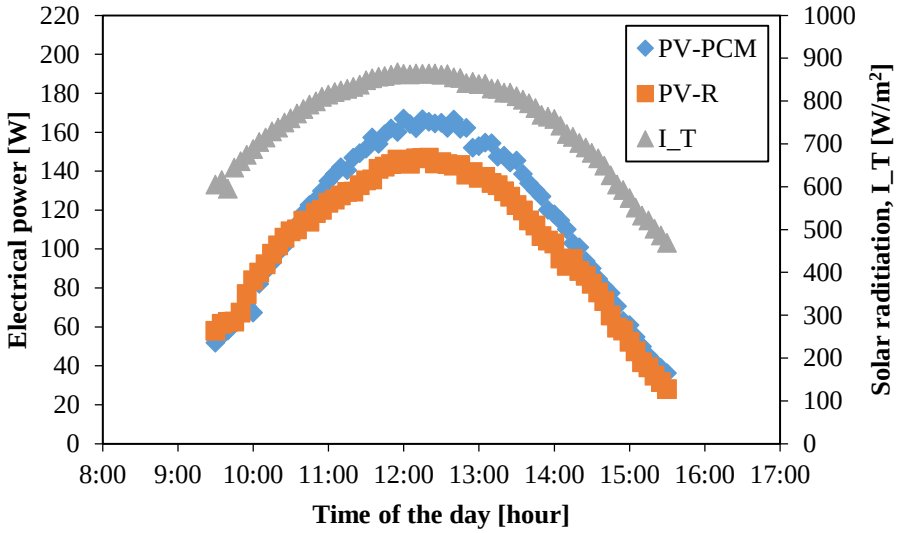


a. Clear sky (December 3, 2015)

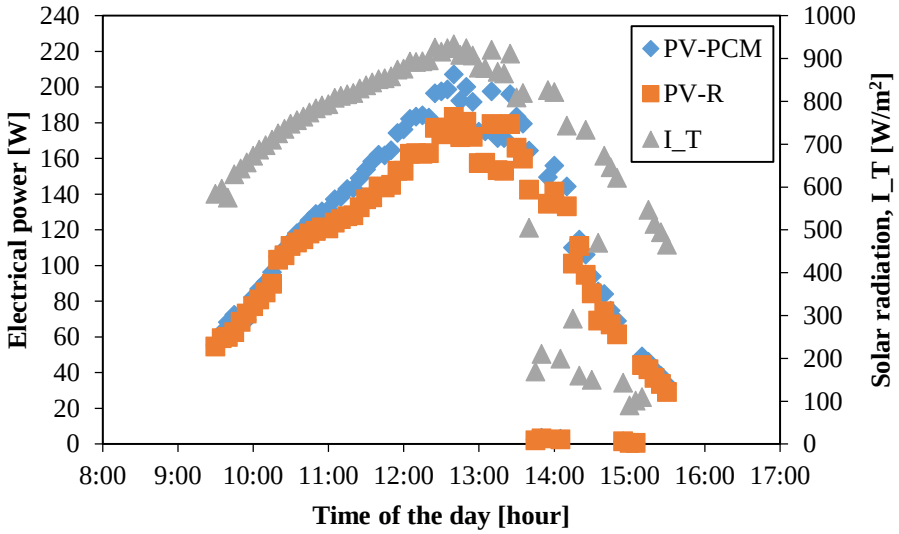


b. Partly cloudy (December 1, 2015)

Figure 4.10 Electrical power on clear sky and partial cloudy day condition.

## 4.6 Correlation of Output Voltage and Output Current

The solar cell was connecting to the external load as illustrated in Figure 4.11. In this picture the optimum voltage and optimum current were collected and electrical generation was obtained. In this section, the correlation of optimum voltage and optimum current as a function of solar radiation and module temperature were found out. The electrical output

was calculated by equation (21). To found out the correlation the MATLAB Programming tool (Surface Fitting Tool) was used.

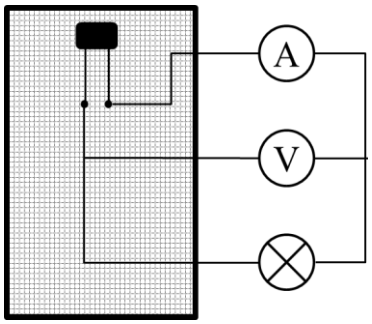


Figure 4.11 Collecting electrical output of solar cell.

### 4.6.1 Output Voltage of Solar Cell

The module solar cell temperature is a main factor affect to the optimum voltage. As indicated in Figure 4.12, more voltage was achieved if the temperature was dropped and in this figure the trend of data shows that the voltage was the second degree of function polynomial with the solar radiation. The correlation of optimum voltage was given in equation 4.1 and its surface fitting was illustrated in Figure 4.13.

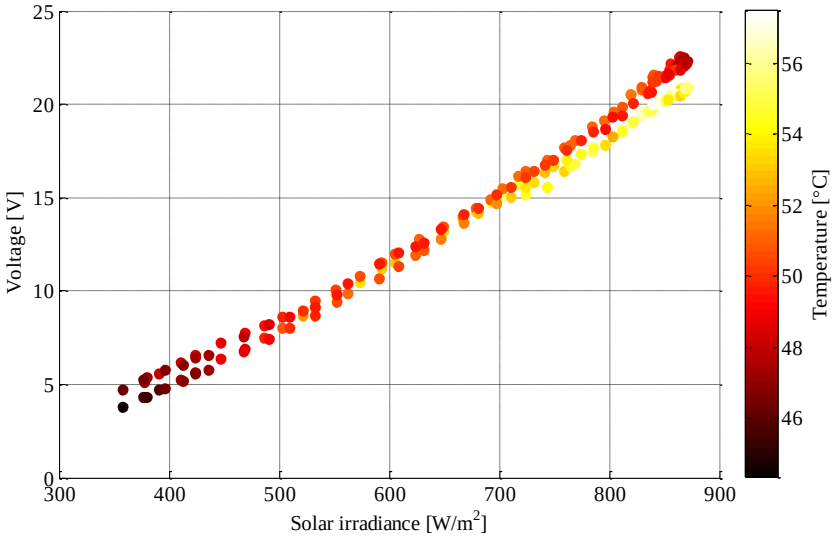


Figure 4.12 Output voltage is function solar radiation and module temperature.

$$V(I_T, T) = p_{00} + p_{10} \cdot I_T + p_{01} \cdot T + p_{20} \cdot I_T^2 + p_{11} \cdot I_T \cdot T \quad (4.1)$$

where,

$p_{00}$ = -15.29 (-22.08, -8.493)
$p_{10}$ = 0.03908 (0.03278, 0.04539)
$p_{01}$ = 0.2582 (0.08905, 0.4273)
$p_{20}$ = 1.853e-005 (1.403e-005, 2.303e-005)
$p_{11}$ = -0.0005386 (-0.0007462, -0.0003309)

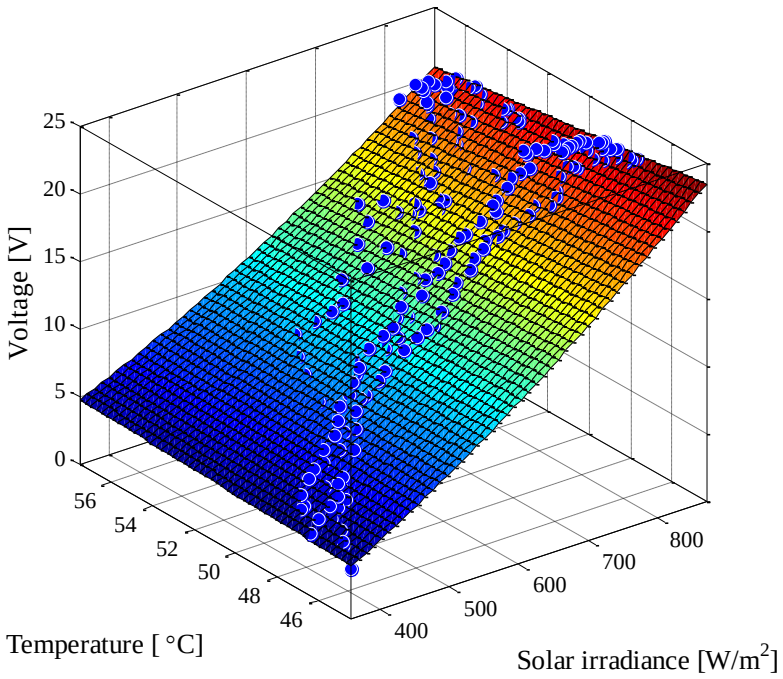


Figure 4.13 3D view of data and fitting curve of optimum voltage, $V(I_T, T)$.

Table 4.2 Goodness of fit of optimum voltage.

| Goodness of fit | Value |
|---|---|
| R-square: | 0.9961 |
| Adjusted R-square: | 0.9961 |
| RMSE: | 0.3561 |

4.6.2 Output Current

The optimum current of solar cell was shown in Figure 4.14. The trend of the optimum current and the solar radiation were the first degree of polynomial function.

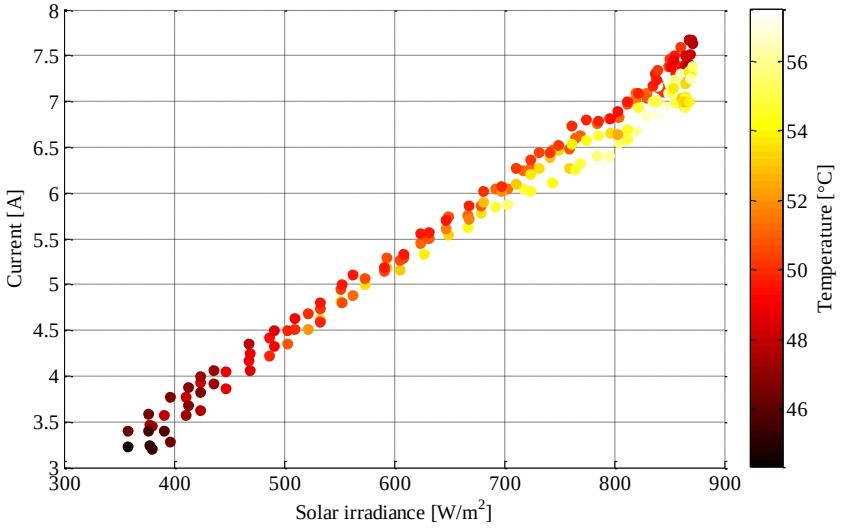


Figure 4.14 Optimum current, solar radiation and module temperature.

$$I(I_T, T) = p_{00} + p_{10} \cdot I_T + p_{01} \cdot T \quad (4.2)$$

where,

$p_{00}$ = 2.196 (1.876, 2.517)
$p_{10}$ = 0.008264 (0.008135, 0.008393)
$p_{01}$ = -0.03843 (-0.04549, -0.03137)

Table 4.3 Goodness of fit of optimum current.

| Goodness of fit | Value |
|---|---|
| R-square: | 0.991 |
| Adjusted R-square: | 0.9909 |
| RMSE: | 0.1213 |

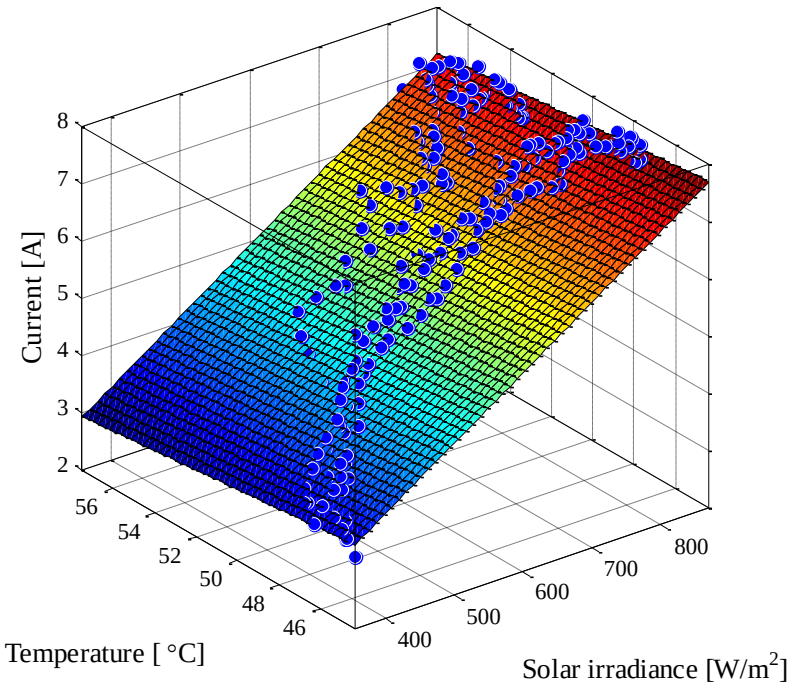


Figure 4.15 3D view of data and fitting curve of optimum current, $I(I_T, T)$.

# Chapter 5
# Long Term Analysis

The main purpose of this chapter was to estimate the unit cost of the electricity generate by solar cell under the Chiang Mai weather condition.

## 5.1 Electrical Generation for Each Month

### 5.1.1 Temperature of Solar Cell Reference

The general equation for predict the solar cell module temperature is calculated from ambient temperature, solar radiation and NOCT following by the equation [31]:

$$T_{PV-R} = T_{\infty} + (NOCT - 20) \cdot \frac{I_T}{800}. \quad (5.1)$$

where, $T_c$ is solar cell reference module temperature. NOCT is normal operating cell temperature. For solar cell EverExceed ESM250-156, NOCT is 45±2 °C. Figure 5.1 shows a validation of simulation with experimental data of solar cell PV-R module temperature on February 15, 2016.

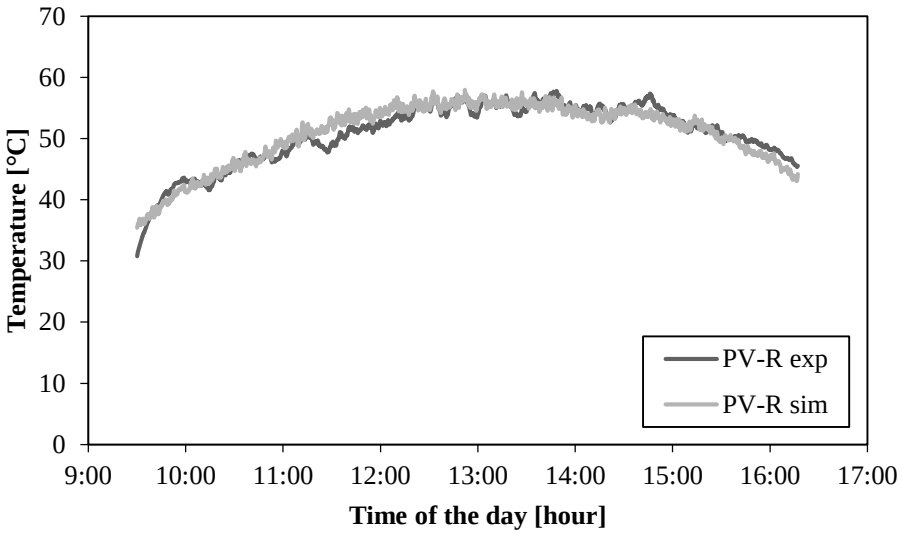


Figure 5.1 Verification of solar cell PV-R module temperature with experimental data (February 15, 2016).

5.1.2 Weather Data

*5.1.2.1 Solar Radiation on Tilt Surface*

The solar radiation is dependent on the sun and earth position. Declination angle of earth is given in:

$$\delta = 23.45sin\left(\frac{2\pi}{365}(DOY - 81)\right). \tag{5.2}$$

The sunset angle is given by

$$\omega_s = \cos^{-1}(-tan(\phi) \cdot tan(\delta)). \tag{5.3}$$

Total daily solar radiation

$$H_o = 24\frac{3600}{\pi}I_{sc}\left(1 + 0.033 \cdot cos\left(2\pi\frac{DOY}{365}\right)\right)\left(cos(\phi)cos(\delta)sin(\omega_s) + \frac{2\pi\omega_s}{360}sin(\phi)sin(\delta)\right). \tag{5.4}$$

The daily diffuse solar radiation ($H_d$) in Thailand is given by Pratinthong [32]

$$\frac{H_d}{H_o} = -4.6408 + 26.5495\left(\frac{H}{H_o}\right) - 28.3422\left(\frac{H}{H_o}\right)^2 - 31.4546\left(\frac{H}{H_o}\right)^3 + 46.4421\left(\frac{H}{H_o}\right)^4 \tag{5.5}$$

$H$ is daily solar radiation for each month in Chiang Mai, Thailand as given in Table 5.1.

The solar radiation on the horizontal plane, $I$ is

$$\frac{I}{H} = \frac{\pi}{24}(a + b \cdot cos(\omega)) \cdot \frac{cos(\omega) - cos(\omega_s)}{sin(\omega_s) - \frac{2\pi\omega}{360}cos(\omega_s)}. \tag{5.6}$$

Where, $a = a_1 + a_2 \cdot sin(\omega_s - 60)$
$b = b_1 + b_2 \cdot sin(\omega_s - 60)$
Hour angle $\omega = 15 \cdot t$

The coefficients $a_1$, $a_2$, $b_1$ and $b_2$ is 0.514, 0.228, 0.512 and 0.083, respectively for Chiang Mai, Thailand [32].

Table 5.1 Average day of the month and average daily solar radiation of each month at Chiang Mai.

| Average day of the month | | | Daily solar radiation, $H$ |
|---|---|---|---|
| Month | Date | Day of the year, DOY | [MJ/m$^2$-day][33] |
| January | 17 | 17 | 17.25 |
| February | 16 | 47 | 19.28 |
| March | 16 | 75 | 21.04 |
| April | 15 | 105 | 20.62 |
| May | 15 | 135 | 19.08 |
| June | 11 | 162 | 16.35 |
| July | 17 | 198 | 15.79 |
| August | 16 | 228 | 17.33 |
| September | 15 | 258 | 17.78 |
| October | 15 | 288 | 16.14 |
| November | 14 | 318 | 15.71 |
| December | 10 | 344 | 18.02 |

The diffuse solar radiation on horizontal surface, $I_d$ is

$$\frac{I_d}{H_d} = \frac{\pi}{24} \cdot \frac{cos(\omega) - cos(\omega_s)}{sin(\omega_s) - \frac{2\pi\omega}{360} cos(\omega_s)}. \quad (5.7)$$

Beam solar radiation, $I_b$

$$I_b = I - I_d. \quad (5.8)$$

The ground albedo, $R_b$

$$R_b = \frac{\cos(\theta)}{\cos(\theta_z)} \quad (5.9)$$

where, $\cos(\theta_z) = cos(\phi) \cdot cos(\delta) \cdot cos(\omega) + sin(\phi) \cdot sin(\delta)$.

$$cos(\theta) = sin(\delta) \cdot sin(\phi) \cdot cos(\beta) - sin(\delta) \cdot cos(\phi) \cdot sin(\beta) \cdot cos(\gamma) + cos(\delta) \cdot cos(\phi) \cdot cos(\beta) \cdot cos(\omega) + cos(\delta) \cdot sin(\phi) \cdot sin(\beta) \cdot cos(\gamma) \cdot cos(\omega) + cos(\delta) \cdot sin(\beta) \cdot sin(\gamma) \cdot sin(\omega). \quad (5.10)$$

Where, $\beta$: Inclination angle

$\gamma$: Surface azimuth angle

$\delta$: Declination angle

$\theta$: Incidence angle

$\theta_z$: Zenith angle

The tilt surface radiation is

$$I_T = I_b \cdot R_b + I_d \cdot \frac{1 + cos(\beta)}{2} + I \cdot \rho_g \cdot \frac{1 - cos(\beta)}{2}. \quad (5.11)$$

The calculation tilt surface solar radiation is determined by the flow as illustrate in Figure 5.2.

*5.1.2.2 The ambient temperature*

The ambient temperature ($T_\infty$) was calculated by

$$T_\infty = \frac{1}{2}\left((T_{max} + T_{min}) + (T_{max} - T_{min}) \cdot \sin(\frac{2\pi}{24}(t - 9))\right) \quad (5.12)$$

Where, $T_{max}$ and $T_{min}$is maximum and minimum ambient temperature as given in Table 5.2.

Table 5.2 The maximum and minimum ambient temperature at Chiang Mai, Thailand.

| Month | Jan | Feb | Mar | Apr | May | Jun | Jul | Aug | Sep | Oct | Nov | Dec |
|---|---|---|---|---|---|---|---|---|---|---|---|---|
| $T_{max}$ | 29.8 | 32.7 | 35.2 | 36.5 | 34.2 | 32.7 | 31.8 | 31.5 | 31.7 | 31.4 | 30.1 | 28.6 |
| $T_{min}$ | 14.9 | 16.2 | 19.5 | 22.9 | 23.8 | 24.0 | 23.9 | 23.7 | 23.2 | 22.2 | 19.2 | 15.7 |

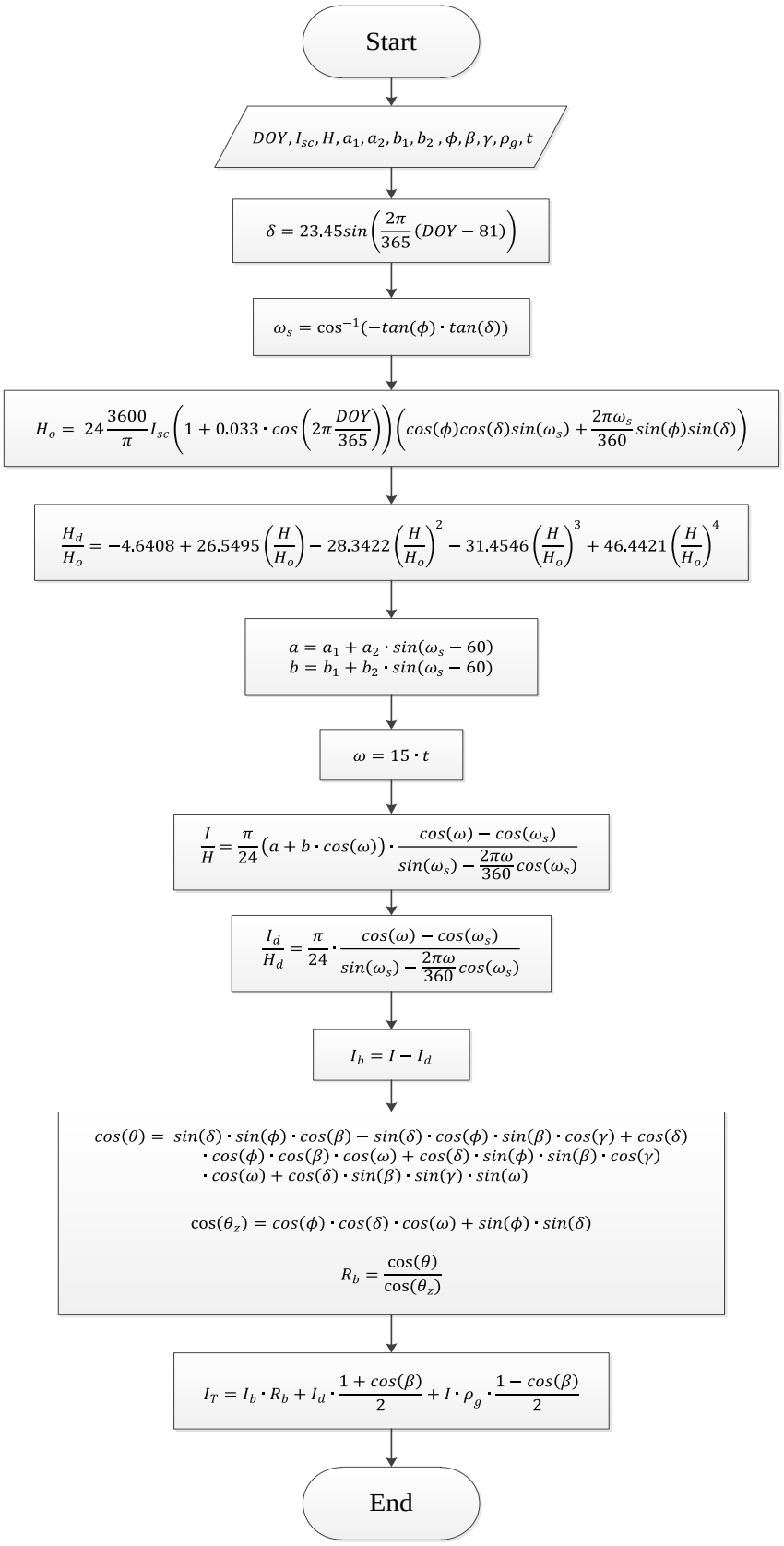


Figure 5.2 Flow chart of simulation to determine tilt surface solar radiation.

5.1.3 Simulation Results

The simulation result of daily electrical energy output of solar cell was given in Figure 5.3. The blue color represents about the solar cell with PCM (PV-PCM) and the red color is the solar cell reference (PV-R). The simulation was taken in 8 hours, from 8:00 to 16:00. The total daily energy on March, April and May is high due the solar radiation sometime was over than 1,000 W/m$^2$. October and November showed the daily energy very low cause by the maximum solar radiation was lower than 800 W/m$^2$.

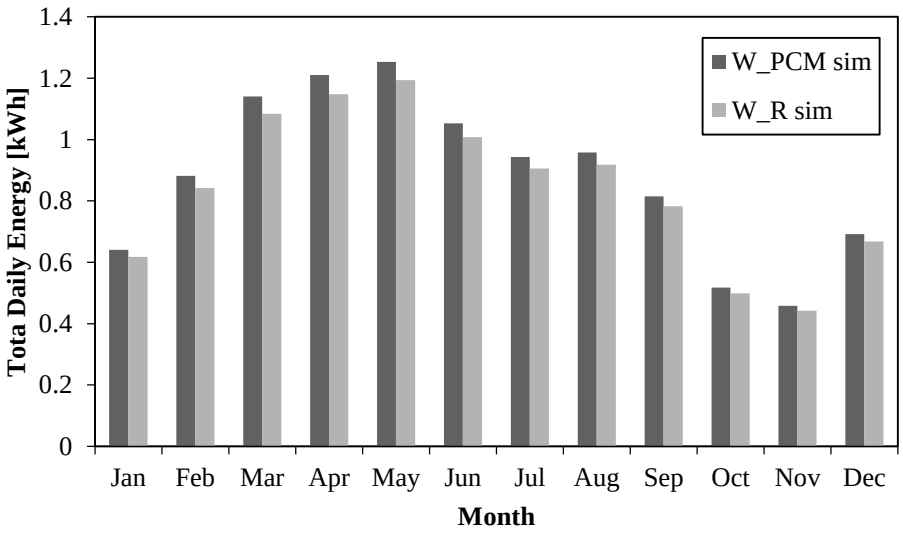


Figure 5.3 Daily electrical energy output of solar cell each month.

## 5.2 Economic Analysis

5.2.1 Conditions for simulation

The solar cell operate 8 hour per day and can generate electricity in whole year and the condition was given in Table 5.3. The expenditure was given in Table 5.4.

Table 5.3 Condition for economic analysis.

| Operating time | 365 days |
|---|---|
| Yearly maintenance cost | 1% of investment cost |
| System life | 25 years |
| Interest rate | i = 6.275% [34] |

Table 5.4 Expenses on materials.

| List of testing material | Expenses |
|---|---|
| Solar cell EMS250- 156 | 17,500 baht |
| Paraffin wax RT42 | 24,765 baht |
| PCM container aluminum | 1,800 baht |
| **Total expenses** | **44,056 baht** |

5.2.2 Unit Cost of electricity

The unit of electricity produce by solar cell with and without PCM was described in this section. The present expenses of the system ($C$) came from initial investment ($C_{inv}$), yearly operation and maintenance cost ($C_{o\&m}$) minus the salvage value ($C_{sv}$) of the system at the present worth.

$$C = C_{inv} + C_{o\&m} - C_{sv}. \tag{5.13}$$

The operating and maintenance cost ($C_{o\&m}$) was 1% of initial investment cost. The salvage value was assumed to be 10% of initial investment cost and as given in the equation:

$$C_{sv} = 0.1 \cdot \frac{C_{inv}}{(1+i)^n}. \tag{5.14}$$

Where, $i$: Discount rate 6.275% [30].

$n$: Service life of the solar cell is 25 years.

The annual expense of the system comes from the conversion of present value to the annual expenses ($C_{an}$).

$$C_{an} = C\frac{i(1+i)^n}{[(1+i)^n - 1]}. \tag{5.15}$$

The unit cost of electricity unity of solar cell was calculated by:

$$C_{product} = \frac{annual\ expenses}{annual\ product\ amount}. \tag{5.16}$$

5.2.3 Simple Payback Period, SPP

Simple Payback Period (SPP) is considered for solar cell with PCM. The result would be used as a basis for investment. The payback period is short, it is the best of investors. Simple Payback Period was calculated by:

$$SPP = \frac{First\ Cost}{Cost\ Saving\ or\ Profit} \quad (5.17)$$

5.2.4 Results

With the daily total electricity generation of solar cell with and without PCM for each month as shown in Figure 5.3, the electricity unit cost was calculated. The solar cell with PCM could produce the electricity in 10.89 Baht/kWh while the solar cell reference was 4.52 Baht/kWh. From the Figure, the annual electrical energy output of solar cell with and without PCM were considered, it were 321.29 and 307.47 kWh/year, respectively. The simple payback period of solar cell with PCM was -12.59 years. From the results, it could be concluded that the reduction of solar cell module temperature with PCM was not so good caused by the electricity unit of solar cell with PCM was higher than the solar cell due to the cost the PCM was higher than price of solar cell 1.5 times as given in Table 5.4.

# Chapter 6
# Conclusions

In conclusion, this work has presented the effect of temperature on the electrical power generation of the solar cell. The using PCM to absorb heat from the solar cell module has been study. The appropriate thick of using PCM for cooling solar cell module has been found out.

## 6.1 Temperature of Solar Cell with and without PCM

An experiment on RT42 PCM was carried out to verify the developed model and the simulated results agreed well with the experiment data. The maximum difference of the module with and without RT42 PCM was around 11 °C and the electrical power could be increased 10% by the unit with the PCM.

## 6.2 Numerical Enthalpy Method

The numerical method using enthalpy method was very good for predicting the thermal model of PCM. The temperature of PCM on 3 days in partly cloudy and 3 days in clear sky of experimental data were used to verify with the simulation results. The simulation results was valid over than 90% which experimental results with deviated ±10%.

## 6.3 Appropriate Thickness of PCMs

With a goodness of model, the finding an appropriate thickness of various commercial PCM was found out. The simulation results showed that the appropriate thickness of PCM with low melting point was thicker than that of PCM with high melting point. RT42 PCM was the best in hot climate like Chiang Mai, Thailand and the appropriate thickness was 4 cm.

## 6.4 Correlation of Output Power of Solar Cell

The correlation of optimum power generation of solar cell was determined by the equation:

$$P = V \cdot I$$

Where, $V$ is optimum voltage which is a correlation of solar radiation and solar cell module temperature was given by:

$$V(I_T, T) = -15.29 + 0.03908 \cdot I_T + 0.2582 \cdot T + 1.853 \cdot 10^{-5} \cdot I_T^2 - 0.0005386 \cdot I_T \cdot T.$$

$I$ is optimum current of solar cell that is also a correlation with solar radiation and solar cell module temperature too

$$I(I_T, T) = 2.196 + 0.008264 \cdot I_T - 0.03843 \cdot T.$$

### 6.5 Unit Cost of Electricity Generate by Solar Cell

With the PCM, the power generate by solar cell was increased but unit cost still expensive due to the cost of PCM was more expensive than the solar cell. The solar cell with PCM could produce the electricity in 10.89 Baht/kWh while the solar cell reference was 4.52 Baht/kWh. The simple payback period of solar cell with PCM was -12.59 years.

### 6.6 Suggestion for Further Research

The direct attach of PCM with solar cell, the extracted heat from the solar cell module was not so good caused by the thermal conductivity of PCM was small. So, Aluminum fin or graphite will be added inside the PCM to enhance the heat transfer, is suggested for the further work. Other recommendation, the amount of PCM will be reduced by putting the PCM in small plastic bag then attach it with rectangular array to the solar cell module.

# References


[1] BP_Global. (2015) BP. [Online]. http://www.bp.com/en/global/corporate/energy-economics/statistical-review-of-world-energy/downloads.html

[2] Climate Change Division US EPA. Overview of Greenhouse Gases. [Online]. https://www3.epa.gov/climatechange/ghgemissions/gases.html

[3] REN21, "RENEWABLES 2014 GLOBAL STATUS REPORT," Paris, ISBN 978-3-9815934-6-4, 2015.

[4] Jesse Geiger, Lars Lisell, and Gail Mosey, "Feasibility Study of Economics and Performance of Solar Photovoltaics at the Ft. Hood Military Base Outside Killeen, Texas," 2013.

[5] Martin K. Fuentes, "A simplified thermal model for flat-plate photovoltaic arrays," Sandia National Labs, Albuquerque, NM (USA), Technical Report SAND-85-0330, 1987.

[6] Geoffrey A. Landis, Danielle Merritt, Ryne P. Raffaelle, and David Scheiman, "High-temperature solar cell development," in 18th Space Photovoltaic Research and Technology Conference, Ohio, 2005, pp. 241-247.

[7] Marc-Alain N. Mutombo , Freddie Inambao, and Glen Bright, "Performance analysis of thermosyphon hybrid photovoltaic thermal collector," Journal of Energy in Southern Africa, vol. 27, no. 1, pp. 28-38, 2016.

[8] E. Radziemska, "The effect of temperature on the power drop in crystalline silicon solar cells," Renewable Energy, vol. 28, no. 1, pp. 1-12, 2003.

[9] M. Abdolzadeh and M. Ameri, "Improving the effectiveness of a photovoltaic water pumping system by spraying water over the front of photovoltaic cells," Renewable Energy, pp. 91-96, 2009.

[10] H. G Teo, P. S Lee, and M. N. Hawlader, "An active cooling system for photovoltaic modules," Applied Energy, pp. 309-315, 2012.

[11] Attakorn Asanakham, Itsarapong Kantiya, and Tanongkiat Kiatsiriroat, "Performance Prediction of Poly-Crystalline Solar Cell Module under Real Practice," Engineering Journal Chiang Mai University, pp. 87-93, 2015.

[12] Patricia Losada-Pérez et al., "Measurements of Heat Capacity and Enthalpy of Phase Change Materials by Adiabatic Scanning Calorimetry," International Journal of Thermophysics, vol. 32, no. 5, pp. 913-924, April 2011.

[13] Harald Mehling and Luisa F. Cabeza, Heat and cold storage with PCM. Berlin: Springer, 2008.

[14] Saffa Riffat, Blaise Mempouo, and Wenbo Fang, "Phase change material developments: a review," International Journal of Ambient Energy, vol. 36, no. 3, pp. 102-115, May 2015.

[15] Someshower Dutt Sharma, Hiroaki Kitano, and Kazunobu Sagara, "Phase change materials for low temperature solar thermal applications," Res. Rep. Fac. Eng. Mie Univ, vol. 29, no. 1, pp. 31-64, 2004.

[16] A. Abhat, "Low temperature latent heat thermal energy storage: Heat storage materials," Solar Energy, vol. 30, no. 4, pp. 313-332, January 1983.

[17] Yongcai Li, Shuli Liu, and Yaqin Zhang, "Experimental Study of the Heat Transfer Performance of PCMs Within Metal Finned Containers," in Progress in Sustainable Energy Technologies Vol II., 2014, ch. 44, pp. 669-684.

[18] Esam M. Alawadhi, "Thermal analysis of a building brick containing phase change material," Energy and Buildings, vol. 40, no. 3, pp. 351–357, January 2008.

[19] Hagar Elarga, Francesco Goia, Angelo Zarrella, Andrea Dal Monte, and Ernesto Benini, "Thermal and electrical performance of an integrated PV-PCM system in double skin façades: A numerical study," Solar Energy, vol. 136, pp. 112-124, October 2016.

[20] Huang, M.J; Eames, P.C.; Norton, B.;, "Thermal regulation of building-integrated photovoltaics using phase change materials," International Journal of Heat and Mass Transfer 47, pp. 2715-2733, 2004.

[21] Biwole, Pascal; Eclache, Pierre; Kuznik, Frederic, "Improve the performance of solar panels by the use of phase-change materials," in World Renewable Energy Congress, Linköping, Sweden, 2011, pp. 2953-2960.

[22] Shivangi Sharma, Asif Tahir, K. S. Reddy, and Tapas K. Mallick, "Performance enhancement of a Building-Integrated Concentrating Photovoltaic system using phase change material," Solar Energy Materials and Solar Cells, vol. 149, pp. 29-39, May 2016.

[23] Sridhar Sadasivam, Fabio Almeida, Dahai Zhang, and Alan S. Fung, "An Iterative Enthalpy Method to Overcome the Limitations in ESP-r's PCM Solution Algorithm," ASHRAE Transactions, vol. 117, no. 2, pp. 100-107, October 2011.

[24] Dariusz Heim and Joe A Clarke, "Numerical modelling and thermal simulation of PCM–gypsum composites with ESP-r," Energy and Buildings, vol. 36, no. 8, pp. 795-805, August 2004.

[25] Frédéric Kuznik, Joseph Virgone, and Kevyn Johannes, "Development and validation of a new TRNSYS type for the simulation of external building walls containing PCM," Energy and Buildings, vol. 42, no. 7, pp. 1004-1009, July 2010.

[26] Y. Zhang, K. Du, J. P. He, L. Yang, and Y. J. Li, "Impact Factors Analysis of the Enthalpy Method and the Effective Heat Capacity Method on the Transient Nonlinear Heat Transfer in Phase Change Materials (PCMs)," Numerical Heat Transfer, Part A: Applications, vol. 65, no. 1, pp. 66-83, January 2014.

[27] S. Armstrong and W.G. Hurley, "A thermal model for photovoltaic panels under varying atmospheric conditions," Applied Thermal Engineering, pp. 1488-1495, 2010.

[28] William S. Janna, Engineering Heat Transfer, 3rd ed., Afshin J. Ghajar, Ed.: Taylor & Francis, 2009.

[29] Curtis O. Pedersen, "Advanced zone simulation in EnergyPlus: incorporation of variable properties and phase change material (PCM) capability," in Proceedings: building simulation 2007, vol. 3, Urbana, 2007, pp. 1341-1345.

[30] (2016, Appril) Rubitherm Technologies GmbH. [Online]. http://www.rubitherm.eu/en/index.php/productcategory/organische-pcm-rt

[31] M. C. Alonso García and J. L. Balenzategui, "Estimation of photovoltaic module yearly temperature and performance based on Nominal Operation Cell Temperature calculations," Renewable Energy, vol. 29, no. 12, pp. 1997-2010, October 2004.

[32] N. Pratinthong, Long Term Simulation of Concrete Solar Collector. Bangkok, Thailand: King Mongkut's Institute of Technology Thonburi, 1996.

[33] Thai Meteorological Department (2014). [Online]. http://www.tmd.go.th/en/

[34] KRUNG THAI BANK. [Online].

http://www.ktb.co.th/ktb/Download/rateFee/RateFeeDownload_4048loan_27_04_59.pdf

[35] Solar cell Rooftop [Online].
http://www.erc.or.th/ERCWeb2/Upload/Document/part3-Solar-Feb%2024%202015-regulation.pdf